Gate Design in Injection Molding of Microfluidic Components Using Process Simulations

Marhöfer, David Maximilian; Tosello, Guido; Islam, Aminul; Hansen, Hans Nørgaard

Published in:
Journal of Micro and Nano-Manufacturing

Link to article, DOI:
10.1115/1.4032302

Publication date:
2016

Document Version
Peer reviewed version

Gate design in injection molding of microfluidic components using process simulations

David Maximilian Marhöfer[1]
Technical University of Denmark
Department for Mechanical Engineering
Produktionstorvet, Building 427A
2800 Kongens Lyngby
Denmark
maxmar@mek.dtu.dk

Guido Tosello
Technical University of Denmark
Department for Mechanical Engineering
Produktionstorvet, Building 427A
2800 Kongens Lyngby
Denmark
guto@mek.dtu.dk

Aminul Islam
Technical University of Denmark
Department for Mechanical Engineering
Produktionstorvet, Building 427A
2800 Kongens Lyngby
Denmark
mais@mek.dtu.dk

Hans Nørgaard Hansen
Technical University of Denmark
Department for Mechanical Engineering
Produktionstorvet, Building 427A
2800 Kongens Lyngby
Denmark
hnha@mek.dtu.dk

[1] Corresponding author.

ABSTRACT

Just as in conventional injection molding of plastics, process simulations are an effective and interesting tool in the area of micro injection molding. They can be applied in order to optimize and assist the design of the micro plastic part, the mold, and the actual process. Available simulation software is however actually made for macroscopic injection molding. By means of the correct implementation and careful modelling strategy though, it can also be applied to micro plastic parts, as it is shown in the present work. Process simulations were applied to two microfluidic devices (a microfluidic distributor and a mixer). The paper describes how the two devices were meshed in the simulations software to obtain a proper simulation model and where the challenges arose. One of the main goals of the simulations was the investigation of the filling of the parts. Great emphasis was also on the optimization of selected gate designs for both plastic parts. Subsequently, the simulation results were used to answer the question which gate design was the most appropriate with regard to the process window, polymer flow, and part quality. This finally led to an optimization of the design and the realization of this design in practice as actual steel mold. Additionally, the simulation results were critically discussed and possible improvements and limitations of the gained results and the deployed software were described. Ultimately, the simulation results were validated by cross-checking the flow front behavior of the polymer flow predicted by the simulation with the actual flow front at different time steps. These were realized by molding short shots with the realized molds and were compared to the simulations at the global, i.e. part level and at the local, i.e. feature level.

***Keywords**: micro injection molding, simulation, meshing, gate design, microfluidic system, short shots.*

INTRODUCTION

The injection molding process is a widely applied and well-established production technology in the industry and accounts for most of today's plastic parts.

Due to its wide spread, it is hence naturally affected by the constant trend of miniaturization towards smaller parts incorporating increasingly more functionality. As a result, the micro injection molding process is commonly seen as one of the key technology of the 21st century for the large-scale and highly automated production of high precision micro structured and three-dimensional parts. The process is capable of yielding net-shaped multi-material plastic parts with complex geometry and diverse functionality. Due to the aforementioned continuous trends of miniaturization of parts and reduction of weight and costs, the field is constantly growing and established for the production of micro products made out of thermoplastics. Furthermore, variations of the process, e.g. micro powder injection molding for metallic and ceramic components or micro two-component injection molding, are in the ascendant. Typical application fields of the micro injection molding process are the medical industry, the telecommunication industry or optics. [1–8]

The miniaturized version of the injection molding process exhibits the same basic process cycle with the following steps [5,9]:

- melting of the plastic granules,
- metering of the molten plastic,
- injection of the material into the cavity of the mold (filling phase),
- packing of the part to compensate for shrinkage,
- cooling to solidification,
- ejection from the mold.

In the field of injection molding, process simulations are based on the method of finite element analysis (FEA). Different software packages such as Autodesk Moldflow®, Moldex3D®, or Sigmasoft® are commercially available on the market. Due to the complexity of the injection molding cycle and equipment, the increasing requirements on the part quality, and the rising number of applications of micro injection molding, process simulations become more and more attractive and relevant. The simulations are carried out because of the same reasons as in other areas of engineering which can be summarized as follows [6,10–15]:

- to assist the part design at an early stage when the molds or tools do not exist yet,
- to avoid costly design errors and subsequently necessary re-engineering actions,
- to shorten the development time and the time-to-market for a new product,
- to eliminate the need or reduce the amount of physical prototyping and experiments,
- to optimize the part and mold design as well as the parameter settings of the manufacturing process,
- to assist the material selection,
- to predict and improve the part quality (e.g. morphology and properties),
- to gain a better understanding of the process characteristics.

In general, commercially available simulation software is – at least up till now – officially made for macroscopic plastic parts and conventional injection molding. The software packages can be applied in micro injection molding to yield qualitatively adequate results, yet the numerical results still lack quantitative accuracy. As a consequence, process simulations are not fully implemented in the process of designing and developing a micro plastic part, although it is state of the art for macro parts. [6,14,16]

First, one reason might be the lack of reliable and comprehensive rheological data and models for the materials, as the data is collected by macroscopic experiments with for micro parts improperly specified boundary conditions, e.g. the no-slip condition at walls which is not necessarily true for micro parts. Additionally, there is the insufficient implementation or handling of microscopically relevant phenomena and particular characteristics of micro parts. This includes the higher surface-to-volume ratio as well as the change and the pressure and viscosity-dependency of the heat transfer coefficient. Both increase the sensitivity to process conditions in the filling, packing, and cooling phases. Also, the higher cooling and shear rates in small cavities lead to different solidification behavior and micro morphology. Besides; the effect of flow hesitation, the microscale rheology, the wettability, the surface tension of the melt can significantly influence the polymer behavior in the micro cavity. [5,6,9,14,17]

Nevertheless, the software tools can yield more precise results for micro parts by using a proper strategy to carefully and comprehensively model and implement the part and the entire injection molding system [9,13,18,19].

Extensive research has been carried out in the field of the application and validation of micro injection molding simulations. However, research is limited to the study of simplified geometries in order to improve the understanding of the performance of simulations on micro cavities. Yet, studies become more advanced and issues and weaknesses of the simulation tools are nowadays clearly identified.

Also, the software manufacturers release new and improved software tools every year, address deficiencies of the software, and claim to achieve more reliable results than previously possible. Encouraged by this development in research and industry, this work attempts to go one step further and focuses on the application of the simulation during the design and engineering process of two complex microfluidic prototype products. The simulations assisted in particular the gate design process of the devices. In addition, the current work presents how the insight coming from the simulations was eventually applied in practice, as the molds were machined based on the simulation results and molded parts were produced.

MICRO FLOW BEHAVIOR

Viscosity

The micro injection molding process consists of the filling, the packing, and the cooling phase. During the filling phase, the plastic flows into the cavity driven by the applied pressure of the injection molding machine. Hence, the plastic's viscosity is of major importance during the filling. According already to Isaac Newton back in 1687, the viscosity was defined as the "lack of slipperiness" of a fluid, i.e. the resistance of the

fluid to deformation [20]. Mathematically, it links the applied shear rate to the shear stress that the fluid experiences. Newtonian fluids show a strictly linear behavior, i.e. the viscosity is independent of the shear rate. In contrast, polymers are non-Newtonian fluids and therefore, the viscosity is a function of the applied shear rate. When polymers experience shear, two effects come into play leading to a decrease in viscosity, the so-called shear thinning: the heat dissipation and the alignment of the polymer chains [21].

The simple power law model is often used for mathematically describing the shear thinning of polymers. The viscosity η is a function of the shear rate $\dot{\gamma}$ and given in the power law model as

$$\eta = m \cdot \dot{\gamma}^{n-1} \tag{1}$$

where *m* and *n* are constants and with $n \leq 1$ generally for polymer melts. This model describes the viscosity well at high shear rates. Nonetheless, injection molding is not only a high shear rate process. The shear rate is highest at the wall of the mold and decreases towards the center of the fountain flow where the shear actually vanishes completely and the polymer melt exhibits the so-called zero-shear rate viscosity.

Consequently, the power law model is insufficient. Instead, the Cross model is widely applied. This model describes the shear rate dependency of the viscosity over a wide range of shear rates very well, because it combines a Newtonian region at low shear rates with a power law shear thinning region at higher shear rates [20]. The viscosity is mathematically given by the Cross model as

$$\eta = \frac{\eta_0}{1 + \left(\frac{\eta_0 \dot{\gamma}}{\tau}\right)^{1-n}} \tag{2}$$

where η_0 is the zero shear rate viscosity and τ is the shear stress. The term $1-n$ describes the slope of the viscosity curve in the power law region, when logarithmically plotted versus the shear rate.

In order to understand and simulate the flow of the polymer during the filling phase, it is however not enough to look only at the viscosity. The applied viscosity model must also account for the temperature changes happening during injection molding. The concept of time-temperature superposition can also be applied to the viscosity. The core of the concept is to shift the known viscosity curve at a reference temperature along the time axis in order to gain the viscosity curve at any temperature different from the reference temperature. The shift factor is given by the Williams-Landel-Ferry (WLF) equation which can be also applied to the zero shear rate viscosity to introduce temperature dependency. This step yields the Cross-WLF model with the zero shear rate viscosity given as

$$\eta_0 = D_1 \exp\left[\frac{-C_1^0\,(T-T_0)}{C_2^0+T-T_0}\right] \tag{3}$$

where D_1, C_1^0, and C_2^0 are constants, T is the temperature, and T_0 is the reference temperature (often the glass transition temperature of the polymer).

Thermodynamics

Besides the viscosity, information about the thermodynamic properties of materials is necessary for computer simulations of the injection molding process. These can be derived from the equation of state of the material which links the pressure, the specific volume, and the temperature. It is therefore also called pvT data [20]. For

plastics, this data is usually provided as pvT diagrams which show the specific volume v as a function of pressure p and the absolute temperature T. The commonly used model for describing the curves of such a diagram is the 2-domain Tait model which is given as [20,22]

$$v(p,T) = v_0(T) \cdot \left[1 - C \ln\left(1 + \frac{p}{B(T)}\right)\right] + v_t(p,T) \tag{4}$$

where $C = 0.0894$ is a constant. The two domains are equal to the solid and molten phase of the plastic which are separated by the transition temperature T_t which is again given as

$$T_t = b_5 + b_6 p. \tag{5}$$

In the lower temperature region, i.e. the solid phase with $T < T_t$, the missing functions of Equation 4 are given as

$$\begin{aligned} v_0(T) &= b_{1s} + b_{2s}(T - b_5), \\ B(T) &= b_{3s} \exp[(-b_{4s}\,(T - b_5)], \\ v_t(p,T) &= b_7 \exp[b_8(T - b_5) - b_9 p]. \end{aligned} \tag{6}$$

Respectively, the upper temperature region, i.e. the molten phase with $T > T_t$, is described by

$$\begin{aligned} v_0(T) &= b_{1m} + b_{2m}(T - b_5), \\ B(T) &= b_{3m} \exp[(-b_{4m}\,(T - b_5)], \\ v_t(p,T) &= 0. \end{aligned} \tag{7}$$

The unknowns $b_{1s}, b_{2s}, b_{3s}, b_{4s}, b_{1m}, b_{2m}, b_{3m}, b_{4m}, b_5, b_6, b_7, b_8$, and $b_9$in the Equations 5-7 are without exception data-fitted coefficients.

Flow

The flow of molten plastics is of anisothermal, compressible, and viscous nature and can consequently be described by the Navier-Stokes equations. The Navier-Stokes equations are a system of non-linear partial differential equations which are the fundamental mathematical model in general fluid dynamics and consist of: the continuity equation (conservation of mass), the momentum equation (conservation of momentum), and the energy equation (conservation of energy). These equations govern also the simulation tools for injection molding. The continuity equation describes the conservation of mass and is commonly given by [23]

$$\frac{\partial \rho}{\partial t} + \boldsymbol{\nabla} \cdot (\rho \boldsymbol{u}) = 0 \tag{8}$$

with the density ρ, and the velocity vector $\boldsymbol{u}$. The momentum equation is commonly formulated as [20]

$$\rho \frac{D\boldsymbol{u}}{Dt} = -\boldsymbol{\nabla} p + \boldsymbol{\nabla} \cdot \boldsymbol{\sigma} + \rho \boldsymbol{g} \tag{9}$$

with the pressure p, the stress tensor $\boldsymbol{\sigma}$, and the gravity vector $\boldsymbol{g}$. Finally, the energy equation, sometimes also referred to as heat-transfer equation, is commonly given as [20]

$$\rho c_p \frac{DT}{Dt} = \beta T \frac{Dp}{Dt} + p \boldsymbol{\nabla} \cdot \boldsymbol{u} + \boldsymbol{\nabla} \cdot (\kappa \boldsymbol{\nabla} T) + \boldsymbol{\sigma} : \boldsymbol{\nabla u} \tag{10}$$

with the specific heat capacity c_p at constant pressure, the absolute temperature T, the coefficient of volume expansion β, and the thermal conductivity κ. Sometimes, the contributions of gravity and inertia in the flow are not considered in simulation software packages or they offer an option to switch the effects on or off.

STUDY CASES

Micro parts

When dealing with micro injection molding, the question arises about what exactly is the definition of “micro” or how small are the parts supposed to be considered in the micro injection molding domain. After some proposals and revisions, three common definitions of different types of micro-molded plastic products nowadays exist [2,3,5,8,24]:

- micro-featured parts with outer dimension in the millimeter range or larger, but locally featuring structures in the micrometer range, typically less than 100-200 µm,
- micro parts with very small outer dimensions, typically 1-2 mm or even entirely in the micrometer range, and shot weights in the order of milligrams,
- parts with larger dimensions, but dimensional tolerances in the micrometer range.

The present work includes two different industrial study cases of the first kind of micro products which will be presented in the following. Both micro plastic parts are of microfluidic nature. In general, the main difference to parts made by conventional injection molding is the aspect ratio, i.e. the thickness-to-lateral dimensions ratio, of the micro part or incorporated micro structures being larger than 1. This means the thickness of the part is often not negligible in comparison to the other dimensions [2].

Microfluidic distributor system

The first plastic part was a microfluidic system which served as distributor of liquid. It is shown as CAD model in Fig. 1. The fluid entered at a single inlet at the top and was then distributed to several outlets at the bottom by a tree-like structure. The part was approximately 25 mm × 7 mm × 2 mm (length × width × height) large. It could be classified as micro plastic part though, as it exhibited micro fluidic structures. The fluidic channels were down to 500 µm wide and less than 200 µm deep. The biggest challenge for this part was the walls separating and limiting the fluidic channels which reached thicknesses down to about 100 µm. The total weight of the part was about 0.25 g (equal to a part volume of approximately 0.19 cm^3).

Process simulations were applied to this plastic part in order to optimize its gate design and position. Therefore, three different gate layouts for the final part at different positions were created (CAD models shown in Fig. 2) and investigated in a first iteration:

- A: fan gate at the long side with a fan width of 25 mm and a minimal fan thickness of 0.5 mm; the total weight and volume of part and feed system were about 0.57 g or 0.45 cm^3, respectively.
- B: fan gate at the short side with a fan width of 7 mm and a minimal fan thickness of 0.5 mm; the total weight and volume of the part and feed system were about 0.50 g or 0.39 cm^3, respectively.

- C: pin gate at the long side with approximated semi-circular cross-section of 0.5 mm diameter; the weight and the volume yielded values of approximately 0.47 g or 0.37 cm^3, respectively.

In a second iteration, the design C was investigated more in detail. The diameter was varied in three steps, namely 0.50 mm, 0.75 mm, and 0.90 mm. The change in gate diameter did not noticeably influence the volume or mass or the model, because of the quite small increase compared to the rest of the part.

The overall flatness of the part was evaluated as major quality criterion of the gate performance. This was because the component was part of an assembly and therefore could not exceed a certain value in flatness. Besides, the process conditions were taken into consideration in order to remain in a suitable process window, ensuring e.g. no excessive shear stress on the polymer, injection molding machine copes with injection pressure and clamping force, sufficient packing, etc. Additionally, the behavior of the polymer flow front was examined, i.e. even filling of the part was required.

The material choice for the final part and hence the simulations in this case was Ultem 1000, a polyetherimide (PEI) grade produced by Sabic, Riyadh, Saudi Arabia. The viscosity and pvT data of the material is shown in Fig. 5 and Fig. 6, respectively. Hence, the melt and mold temperature were chosen accordingly at 380 °C and 160 °C, respectively. The part was supposed to be molded on an injection molding machine of type Allrounder 370 A 600-70 made by Arburg, Loßburg, Germany, with a screw diameter of 18 mm and a maximum clamping force of 60 tons. This machine was thus

chosen for the simulations. The machine speed was automatically determined by the software in order to reach a target filling time in the simulation of 0.4 s.

The material choice for the experimental short shots was the polypropylene (PP) BJ356MO produced by Borealis, Vienna, Austria. The melt temperature was accordingly set to 230 °C, whereas the mold temperature was kept at 40 °C. The injection speed was set to 75 mm/s. The used injection molding machine was the same as for the simulations.

Microfluidic mixer system

The second plastic part was also a micro fluidic device and serves as a mixer. In addition to the actual part, a feed system consisting of a film gate, runner, and sprue was designed. The part and the part with feed system are shown as CAD model in Fig. 3 and Fig. 4. The device itself had outer dimensions of about 20 mm × 20 mm × 2 mm (length × width × height). Alike the first part, it was in fact a micro part because of the microfluidic features. The channel depth was between 300 µm and 600 µm, the width less than 1 mm, and the wall thickness about 400 µm. The pillars in the center of the part were the most prominent micro features. They were about 600 µm high and 200-250 µm in diameter and had thus an aspect ratio of about three. The part weight was about 0.54 g (equal to a volume of approximately 0.54 cm^3); the total weight including the feed system was about 2.3 g (equal to a volume of about 2.3 cm^3).

The simulation results were evaluated with regard to overall filling pattern and the filling of the micro pillars. Furthermore, the thickness of the film gate was varied and

set to three different values (280 µm, 420 µm, and 560 µm). The part weight did not noticeably differ between the three gate configurations. The three layouts were evaluated based on the filling characteristics of the polymer, e.g. flow, shear stress, temperature, packing performance, shrinkage, etc.

The material choice for the final part and thus the simulations was a cyclic olefin copolymer (COC): Topas 5013L-10 produced by Topas Advanced Polymers, Frankfurt am Main, Germany. The viscosity and pvT data of the material is shown in Fig. 7 and Fig. 8, respectively. The melt and mold temperature in the simulation were set to typical practical processing settings for COC of 280 °C and 110 °C, respectively. The part was supposed to be molded on the same aforementioned machine Arburg Allrounder 370 A 600-70. In this case, the filling was set to be velocity controlled with an injection speed of 200 mm/s.

The material choice for the conducted experimental short shots was the polypropylene (PP) Sabic PP 579S. The melt temperature was set to 230 °C, the mold temperature was set to 60 °C, and the injection speed of the machine was chosen as 40 mm/s. For the short shots, the same injection molding machine was deployed as for the simulation.

SIMULATION SOFTWARE AND MODELS

Software properties

In this work, the commercially available software tool Autodesk Simulation Moldflow Insight® (ASMI) in the version of 2014 and 2015 made by Autodesk, San

Rafael, USA, was used for carrying out the process simulations. The software enables to investigate the whole injection molding cycle with the filling, packing, and cooling phases, the mold and part behavior during the process, and also the quality of the resulting plastic part, e.g. with regard to the shrinkage and warpage behavior.

Due to the complexity of the process and the geometries of injection molding, the mathematical models describing the physics are impossible to be solved directly for an entire plastic part. Therefore, ASMI is a finite element analysis (FEA) based software, like most of the commercial tools for the investigation and simulation of the injection molding process. The FEA breaks down the original geometry into smaller entities. This discretization of the geometry in elements is called meshing. The mesh consists of triangular elements given by three nodes in case of 2D analyses. In 3D on the contrary, the geometry is represented by tetrahedral elements given by four nodes. For each node, the mathematical models can be simplified and together with some reasonable approximations, the equations can be solved individually for every node. In the sum, this yields a solution for the entire investigated geometry.

In general, the accuracy of the approximated solution given by the FEA depends on the density of the mesh. Hence, the finer the mesh, the more accurate the solution will be. However, the finer the mesh, the more equations have to be solved because of the higher number of nodes and thus the longer the computation time of the conducted simulation will be.

ASMI applies the meshing together with the Cross-WLF and Tait model to describe the viscosity and pvT behavior of the plastics. The flow is modeled by the

aforementioned Navier-Stokes equations in 3D meshes and by the generalized Hele-Shaw model in 2D meshes. The flow of the plastic starts at one or several nodes which were chosen as the injection location. From there, the flow advances to more and more neighboring nodes in every time step until the entire meshed plastic part is completely full or the material flow freezes completely.

Regarding the Navier-Stokes equations, ASMI provides the option to turn on the effect of gravity and inertia which were enabled in this simulation study.

Simulation models

The used simulation models were related to the actual plastic part with the feed system. The meshing of both entities in ASMI was based on the original and imported CAD data and conducted in process with two successive steps. First, the meshing was done in the two-dimensional domain, leading to a surface mesh of the part. Afterwards, the surface mesh was maintained and the volume of the part was meshed in the 3D domain with tetrahedral elements. The meshing and simulation settings varied between the two products, but they were kept equal among the gate configurations of each study case.

Due to the large differences in size of the incorporated features (e.g. sprue and micro channels for the distributor or sprue and micro pillars for the mixer), a so-called multi-scale mesh was applied to both study cases, i.e. the mesh size can vary significantly between the various meshed entities, but also within one meshed part.

The mesh intensifies at the micro structures in order to capture the actual CAD geometry and to provide sufficient resolution to prevent from effects given by the mesh like a Boolean behavior of the filling where the structure is empty in one time step and in the next time step it is completely filled, but an intermediate step is not possible.

The mesh size for the microfluidic distributor ranges from 40-800 µm edge length of the tetrahedral elements for all three configurations (design A, design B, and all gate sizes of design C). This results in models with approximately 2.9-3.8 million tetrahedrons. The model of gate design C is exemplary shown in Fig. 9. The remarkable difference in element count is caused by the very different volumes (compare to previous section) and shapes of the three gate types.

The multi-scale mesh of the microfluidic mixer (shown in Fig. 10) comprises mesh sizes in the order of 65-800 µm for all gate thicknesses, resulting in models with 4.0-4.2 million tetrahedral elements. The volume difference of the three gate configurations is negligible. However, the necessity for decreasing mesh size with decreasing film gate thickness leads to the difference in element count.

RESULTS AND DISCUSSION

For both plastic products, the simulations showed that all examined gate designs provided complete filling of the respective part. No short shots were detected. The important simulation results for both parts are summarized in Table 1 and Table 2.

Microfluidic distributor system

Regarding the microfluidic distributor and as listed in Table 1, all three gate designs result in similar injection times of about 0.4 s and thus go in accordance with the demanded, optimum injection time.

Moreover, the pin gate requires as expected the highest maximum injection pressure with about 95 MPa because of its narrow cross-section. Still, it is clearly within the limits of the machine capability, the maximum clamping force likewise. On the other hand, design A requires the lowest injection pressure with about 51 MPa due to the large cross-section of the long fan gate.

The filling behavior of the polymer is illustrated in Fig. 11 for one single time step during the filling phase. Design A shows clearly the most inhomogeneous filling, whereas B and C yield more even flow fronts. When looking at the entire filling phase design C is slightly in favor over design B regarding the flow front.

The reason for this inhomogeneous filling in design A is the flow length from the sprue to the actual cavity. It is much smaller in the center of the gate than at the outer flanks, so that the flow reaches the cavity much earlier in the center. Design B shows however that a fan gate makes an even distribution of the material flow in the center and at the flanks leading to an even flow front entering the cavity.

The observed flow disturbances in the cavity which lead there to the uneven flow front are caused by the ribs and the significant thickness variation of the part. All ribs are introduced in the first place to minimize the warpage of the part and provide stabilization. The ribs are thinner than the actual bulky body, and therefore they act as flow restrictors where the flow front lags behind, as it is illustrated in Fig. 12.

The thickness variation along the part (depicted in Fig. 13) has a similar effect. The plastic flow will be restricted in thinner areas and flow more quickly where the party is thicker. The depressions between the ribs show only about one third of the total part thickness and restrict the flow. In contrast, the fluidic channel areas exhibit more than three quarter of the total thickness and thus act as flow leader in direct comparison.

The inhomogeneity in the flow front and the difference in flow direction between the three investigated designs also affect the warpage of the plastic part which can be predicted by the simulations. The warpage of this part is crucial, as the flatness is directly connected to it and one of the major part quality criteria at the same time. The results for the warpage prediction of the simulations for all three gate designs are shown in Fig. 14.

Design A shows the worst warpage behavior which is best seen in z direction (Fig. 16). The inverse “U-shape” is very distinct and the warpage level is also highest indicated by the quite strong red area in the center.

Design B shows worse warpage than design C which is best seen by looking at the deflection of the lower left corner in z direction. It bent up more significantly when compared to design C. In addition, the warpage in y direction (Fig. 15) for design B was the most unsymmetrical.

With regard to the average shrinkage, design B gives the lowest value. The maximum shear rate of gate design C exceeds plainly the recommended limit for the chosen polymer. Thus, there is a risk for material degradation. However, only design C

fulfills the requirement of a flatness value below 10 µm. Altogether, gate C seems the most favorable choice.

As a first option, the shear stress can be lowered by modifying the cross-section of the pin gate. Derived from runners, a full round or trapezoidal shape is more efficient, i.e. causing lower pressure drop and shear. The excessive shear stress was counteracted in this work alternatively by simply increasing the width of the pin gate which was the reason for the second iteration of the microfluidic distributor.

The maximum shear rate decreased from the aforementioned 104 000 s^{-1} for the 0.50 mm thick gate (compare to Table 1) to values of 54 000 s^{-1} and 20 000 s^{-1} for the 0.75 mm and 0.90 mm, respectively. The two latter values are fairly below the permitted maximum level of 50 000 s^{-1}.

The warpage results in z direction for the three different gate sizes are shown in Fig. 17. The thinnest gate with 0.50 mm diameter shows the greatest warpage, the thickest gate with 0.90 mm diameter shows the smallest warpage. This can be noticed in Fig. 13 especially at the upper left corner in red and the lower right corner in green which are much more emphasized for the thin gate. The reason for this is probably the better packing performance of the thick gate which freezes later than the thin and medium-sized one, allowing for larger and longer shrinkage compensation.

In conclusion, the increase in gate diameter does not only enable to push the maximum shear rate to an acceptable level, but it is even beneficial for further improvement of the flatness of the microfluidic distributor.

The design of the prototype was finalized including the pin gate at the long side of the part with a diameter of 0.9 mm and indeed realized as actual cavity in a steel mold. Hence, the insight coming from the simulation could be applied in practice. The final mold which was used for part production and the short shots is depicted in Fig. 18.

Flow pattern validation of microfluidic manifold

The comparison between the actual flow front given by short shots molded in PP and the predicted flow front given by the simulation is done on a qualitative basis. The comparison of the flow fronts on part level is illustrated in Fig. 19. The overlay of the simulated and real flow front shows good agreement between the flow fronts. Hence, the simulation can forecast the actual flow front behavior. However, there is some small deviation to observe: the flow front given by the simulation is slightly ahead in the lower half of the cavity, whereas it lags slightly behind in upper half of the cavity compared to the short shots.

The comparison of the flow fronts on feature level looking closer at the micro features of the microfluidic manifold is shown in Fig. 20. Also, time steps can be found in the simulation which show good agreement to the actual part shape. Nevertheless, the simulation predicts falsely the filling of the micro features. None of the real parts shows complete filling of the micro features which most likely happens later at the end of the filling phase or in the packing phase. The simulation on the other hand shows complete filling already at an early stage of the filling phase.

Moreover, it should be noted that for the single short shots the time step for the best fit of the flow front on part level often differs from the time step for best fit on feature level. The differences are in the range of up to about 3 % of the individual filling time. This divergence might be explained by the fact that the simulation assumes perfect venting, since the mold is not modelled. In reality, the air has to escape from the micro features of the cavity and the built up counterpressure holds the plastic flow back.

Microfluidic mixer system

The film gate is in general well suited for the part, as the polymer flow enters the cavity rather uniformly across the gate width, as depicted in Fig. 21. Additionally, the simulation identifies hesitation of the polymer flow at the micro pillars which is illustrated in Fig. 22. It is characterized by the easier flow into the bulky substrate (in the actual main flow direction) than into the micro pillars. The hesitation effect is a common phenomenon for cavities of different thicknesses, as it is pronouncedly the case for micro structures on substrates. [24]

This leads to the flow actually reaching the end of the cavity before the micro pillars are completely filled which has to be considered for setting up the packing phase when producing the part.

The volumetric shrinkage for all three gates is depicted in Fig. 23 and listed in Table 2. The thickest gate proved to achieve the lowest volumetric shrinkage, highest part mass (mass increase due to larger gate thickness is negligible), and thus the best

packing performance. In addition, the shrinkage is also quite homogenous compared to the thinnest gate. Even and low shrinkage is important, as the part will be assembled to another part by means of the four holes. Any displacement or misalignment will make the assembly more difficult.

As shown in Table 2, the shear rate is at an acceptable level for the thickest gate only, whereas for the small and medium gates the risk of polymer degradation exists. On the other hand, it also needs the highest clamping force which can however be delivered by a typical injection molding machine without problems.

The injection pressure yields no such clear and simple trend. With values of 35.5 MPa and 35.1 MPa, the gates sizes of 280 µm and 560 µm do not show a significant pressure difference. For the medium-sized gate however, the predicted injection pressure of 30.8 MPa is noticeably lower (about 12 %) in comparison.

In general, it can be assumed that injection molding exhibits high pressure domains. At very high pressures, the bulk compression of the polymer melt decreases the free volume which again leads to a reduction of the mobility of the polymer chains. This effect is known as that the so-called pressure-induced viscosity increase. [25]

The non-linear behavior of the injection pressure could thus be explained by taking three effects into consideration: the pressure drop to drive the flow, the pressure-induced viscosity increase, and the shear thinning effect of polymers.

At the small gate, the pressure drop is large; the pressure-induced viscosity increase counteracts the shear thinning effect. In total, the injection pressure is hence high. In case of the medium-sized gate, the pressure drop and the pressure-induced

increase in viscosity get less. The shear thinning becomes visible, and the total injection pressure is thus lower. The injection pressure rises again for the large gate, because the shear thinning effect disappears. In the aggregate, the pressure drop and pressure induced viscosity are more pronounced.

Eventually, the mold of the prototype was realized and one of the mold inserts used for the actual part production and the short shots is shown in Fig. 24. Implementing the findings of the simulations in the tooling, the final design incorporates the film gate with 560 μm thickness.

Flow pattern validation of microfluidic mixer

Similar to the microfluidic manifold, the comparison between the actual flow front given by short shots in PP and the predicted flow front given by the simulation is done on a qualitative basis. The comparison of the flow fronts on part level is illustrated in Fig. 25. The overlay of the simulated and real flow front shows also in this case good agreement between the flow fronts with minimal deviations. The simulation can forecast the actual flow front behavior more accurately than in case of the manifold. The reason is possibly that the mixer exhibits a lower thickness variation which distorts the flow.

The comparison of the flow fronts on feature level looking closer at the micro pillars of the microfluidic mixer is shown in Fig. 26. First, the effect of a depression at the base of the pillars should be noted in the plastic samples. Probably, they are caused by air in the cavity which creates a counterpressure and leaves an imprint. This effect could

be seen for all pillars. Although the simulation assumes perfect venting, the plastic flow also showed narrow depressions at the base shortly before flowing into the pillars.

Despite the fact that the match for the flow front on part level was better, the filling of the micro pillars was predicted with less accuracy than in case of the microfluidic manifold. In the simulation, the pillars fill too early; likely for the same reason mentioned before for the manifold: the simulation assumes an evacuated mold, whereas in reality the air might cause a counterpressure in the pillars which holds back the plastic flow. Additionally, the time steps in the simulation giving the best fit on part level or respectively on the feature level (considering pillars and walls, since the filling of the pillars were not predicted correctly) show differences of up to about 1 %.

CONCLUSION

The simulation-aided optimization of the gate design and the gate layout of two microfluidic plastic components was successfully conducted by using Autodesk Moldflow. The investigations included the behavior of the polymer flow during the filling phase and several part quality criteria, e.g. shrinkage and warpage. The simulation of the parts was based on the application of a multi-scale mesh with a large span of mesh element size with 3D tetrahedral elements to the part and the entire feed system. The decision on the final gate for both parts was based on comparison between the simulated performances of the different given gate layouts.

Three different gate types were evaluated for the microfluidic distributor. For this device, the gate optimization yielded the gate type and the gate size. The pin gate proved to be the best gate choice. However, the gate size had to be carefully selected and increased to 0.9 mm, as the maximum shear stress of the polymer was easily exceeded with the default size.

The thickness of the film gate of the microfluidic mixer was investigated, and the results showed that the thickest gate provides superior performance. The simulation proved the suitability of the film gate and the hesitation of the polymer flow at the micro pillars as the most challenging features of the part.

Nonetheless, the simulation results showed also some inconsistency regarding the injection pressure. Their cause is not entirely clear, possibly the limited capability of the simulation software to handle micro plastic parts and micro scale phenomena. It is important to keep in mind that such limitations do exist and simulation results of micro injection molding should always be critically analyzed.

With this work, it was furthermore shown that the simulation of the injection molding process is a supportive and effective tool for micro manufacturing and the design of micro plastic components. It was used for the part validation by checking, if the required part quality and possible tolerances are reached. Besides, the part and tool design was assisted by finding the most suitable gate type and size without spending lots of effort on prototyping and molding trials with different gate geometries. Finally, the insight of the simulations was in fact applied in practice by machining the cavities for both devices based on the findings in the simulation.

Simultaneously, it could be checked whether the given process parameters were suitable for reaching the required part quality as well as for successful molding or if problems or defects were to be expected.

The presented work also included the validation of the simulation by cross-checking with the actually molded plastic components made out of PP in order to find out how good the prediction actually was. It was observed that the simulation could predict the flow fronts on the global part level well, but the flow prediction on the local feature level showed some divergence to reality. In general, the simulation yielded an unproblematic and too early filling of the micro features of both prototypes.

Simulations easily allow changing the material of the part in order to see whether other plastics could be deployed for the study cases, as the chosen polymers are rather expensive. Possible improvements and enhancements of the simulations comprise the implementation of a more comprehensive model including the actual steel mold block and different layouts of the heating/cooling system. In general, the final influence of the mold and cooling on the part quality can be investigated by doing so. The cooling circuit can be optimized still in the design phase before the actual production of the mold starts. Finally, simulation results can benefit also from taking into account the effect of mold venting in connection with the clamping force, the surface finish of the plates, and the actual air gap at the mold closure parting plane.

ACKNOWLEDGMENT

This paper reports work undertaken in the framework of the project “Hi-MICRO” (High Precision Micro Production Technologies, http://www.hi-micro.eu/), Task 1.2: Micro Injection-Moulding Oriented Product Design. Hi-MICRO is a collaborative project supported by the European Commission in the 7th Framework Programme (Grant agreement no: 314055). Contribution from the Hi-MICRO consortium which provides the study cases for the application of the simulations in the presented work is acknowledged.

REFERENCES

[1] Attia, U. M., and Alcock, J. R., 2011, "A review of micro-powder injection moulding as a microfabrication technique," J. Micromechanics Microengineering, **21**(4), p. 043001.

[2] Giboz, J., Copponnex, T., and Mélé, P., 2007, "Microinjection molding of thermoplastic polymers: a review," J. Micromechanics Microengineering, **17**(6), pp. R96–R109.

[3] Zhiltsova, T. V., Oliveira, M. S. A., and Ferreira, J. A., 2013, "Integral approach for production of thermoplastics microparts by injection moulding," J. Mater. Sci., **48**(1), pp. 81–94.

[4] Tada, K., Fukuzawa, D., Watanabe, A., and Ito, H., 2010, "Numerical simulation for flow behaviour on micro- and nanomoulding," Plast. Rubber Compos., **39**(7), pp. 321–326.

[5] Yang, C., Yin, X.-H., and Cheng, G.-M., 2013, "Microinjection molding of microsystem components: new aspects in improving performance," J. Micromechanics Microengineering, **23**(9), p. 093001.

[6] Nguyen-Chung, T., Loser, C., Juttner, G., Pham, T., Obadal, M., and Gehde, M., 2011, "Simulation of the micro-injection moulding process: effect of the thermo-rheological status on the morphology," Proc. Inst. Mech. Eng. Part E J. Process Mech. Eng., **225**(4), pp. 224–238.

[7] Drummer, D., and Messingschlager, S., 2014, "Ceramic injection molding material analysis, modeling and injection molding simulation," Proceedings of the 29th International Conference of the Polymer Processing Society (PPS), pp. 582–586.

[8] Griffiths, C. A., Dimov, S. S., Scholz, S. G., Hirshy, H., and Tosello, G., 2011, "Process factors influence on cavity pressure behavior in microinjection moulding," **133**(June 2011).

[9] Drummer, D., Ehrenstein, G. W., Hopmann, C., Vetter, K., Meister, S., Fischer, T., Piotter, V., and Prokop, J., 2012, "Innovative Prozesstechnologien für die Herstellung thermoplastischer Mikrobauteile - Analyse und vergleichende Bewertung," Zeitschrift Kunststofftechnik (Journal Plast. Technol., **8**(5), pp. 440–467.

[10] Costa, F. S., Tosello, G., and Whiteside, B. R., 2009, "Best practice strategies for validation of micro moulding process simulation," Proceedings of the Polymer Process Engineering 2009 Conference, pp. 259–261.

[11] Vietri, U., Sorrentino, A., Speranza, V., and Pantani, R., 2011, "Improving the predictions of injection molding simulation software," Polym. Eng. Sci., **51**(12), pp. 2542–2551.

[12] Khalilian, S. A., Park, S. S., and Freiheit, T. I., 2013, "The Application of Commercial Injection Molding Software to Micro-Component Design and Process Development," Proceedings of the 8th Internation Conference on Micro Manufacturing (ICOMM 2013 No. 59), pp. 50–56.

[13] Marhöfer, D. M., Tosello, G., Hansen, H. N., and Islam, A., 2013, "Advancements on the simulation of the micro injection moulding process," Proceedings of the 10th International Conference on Multi-Material Micro Manufacture (4M 2013), Research Publishing Services, pp. 77–81.

[14] Tosello, G., Gava, A., Hansen, H. N., Reinecke, H., Lucchetta, G., and Schoth, A., 2009, "Experimental validation of micro molding simulations using different process setting conditions," 67th Annual Technical Conference (ANTEC) of the Society of Plastics Engineers 2009, Chigago, IL, pp. 1787–1793.

[15] Chen, L., Kietzmann, C., Astbury, D., and Shao, L., 2014, "Advanced cooling simulation technologies for the injection molding process," p. 8.

[16] Cramer, A., Michaeli, W., Friesenbichler, W., and Duretek, I., 2007, "Simulation des Spritzgießprozesses von Mikrobauteilen," Zeitschrift Kunststofftechnik (Journal Plast. Technol., **3**(1), pp. 1–26.

[17] Young, W. B., 2005, "Simulation of the filling process in molding components with micro channels," Microsyst. Technol., **11**(6), pp. 410–415.

[18] Tosello, G., Costa, F. S., and Hansen, H. N., 2011, "Micro Injection Moulding High Accuracy Three-Dimensional Simulations and Process Control," Proceedings of Polymer Process Engineering 11: Enhanced Polymer Processing, Bradford, p. 14.

[19] Islam, A., Hansen, H. N., Marhöfer, D. M., Angel, J., Dormann, B., and Bondo, M., 2012, "Two-component micro injection moulding for hearing aid applications," Int. J. Adv. Manuf. Technol., **62**(5-8), pp. 605–615.

[20] Kennedy, P., and Zheng, R., 2013, Flow Analysis of Injection Molds, Hanser, Munich.

[21] Griffiths, C. A., Dimov, S. S., Brousseau, E. B., and Packianather, M. S., 2008, "The finite element analysis of melt flow behaviour in micro-injection moulding," Proc. Inst. Mech. Eng. Part B J. Eng. Manuf., **222**(9), pp. 1107–1118.

[22] Wang, J., 2012, Some critical issues for injection molding, InTech, Rijeka, Croatia.

[23] Bruus, H., 2008, Theoretical Microfluidics, Oxford University Press, Oxford.

[24] Attia, U. M., Marson, S., and Alcock, J. R., 2009, "Micro-injection moulding of polymer microfluidic devices," Microfluid. Nanofluidics, **7**(1), pp. 1–28.

[25] Lenk, R. S., 2012, Polymer Rheology, Springer Science & Business Media, New York.

[26] Autodesk, 2015, "Autodesk Simulation Moldflow Insight 2015."

Figure Captions List

Fig. 1 CAD model of the first investigated micro plastic part with tree-like structure for the distribution of fluid (highlighted in blue color).

Fig. 2 CAD models of the microfluidic distributor with three different gate designs.

Fig. 3 CAD model of the second investigated micro plastic part which acts as microfluidic mixer.

Fig. 4 CAD model of the second investigated micro plastic part with feed system (film gate, runner, sprue).

Fig. 5 Viscosity versus shear rate at different temperatures of the PEI Ultem 1000 which was used for the microfluidic manifold [26].

Fig. 6 pvT data at different pressure levels of the PEI Ultem 1000 which was used for the microfluidic manifold [26].

Fig. 7 Viscosity versus shear rate at different temperatures of the COC Topas 5013-L10 which was used for the microfluidic mixer [26].

Fig. 8 pvT data at different pressure levels of the COC Topas 5013-L10 which was used for the microfluidic mixer [26].

Fig. 9 Meshed micro distributor with closer view on some details (micro walls at outlets). Range of mesh edge length of the entire model: 40-800 µm.

Fig. 10 Meshed micro mixer with closer view on some details (micro pillars and rim). Range of mesh edge length of the entire model: 65-800 µm.

Fig. 11 Filling behavior for the three configurations of the fluidic distributor.

Fig. 12 Example of a rib acting as flow restrictors and causing the flow to lag behind compared to the bulk of the microfluidic distributor.

Fig. 13 Thickness variation in the part which contributes to the disturbance of the flow front in the cavity during the filling phase of the microfluidic distributor.

Fig. 14 Warpage prediction of the simulation in x direction for the micro fluidic distributor.

Fig. 15 Warpage prediction of the simulation in y direction for the micro fluidic distributor.

Fig. 16 Warpage prediction of the simulation in z direction for the micro fluidic distributor.

Fig. 17 Prediction of the warpage in z direction for the different gate sizes of gate design C (pin gate) of the microfluidic distributor.

Fig. 18 Actual steel mold of the microfluidic manifold with stationary half (left) and the movable half (right). The cavity was machined according to the optimized design based on simulation results applying the insight from the simulations in practice.

Fig. 19 Comparison on part level by overlay of the actual flow front given by short shots molded in PP and the simulated flow front for the microfluidic manifold.

Fig. 20 Comparison on feature level between SEM picture of the actual flow front given by short shots in PP (left) and the simulated flow front (right) for the microfluidic manifold.

Fig. 21 Film gate of the microfluidic mixer with quite even flow front when the plastic is entering the actual part cavity.

Fig. 22 Cross-sectional view of the flow in the microfluidic mixer with indication of the distinct hesitation effect at the micro pillars: the filling in bulk direction is faster than in the direction of the micro pillars, i.e. the flow length *a* in bulk direction is larger than the flow length *b* in direction of the micro pillars.

Fig. 23 Average volumetric shrinkage for the three film gates of the microfluidic mixer.

Fig. 24 Finished mold insert of the microfluidic mixer. The cavity design was machined accordingly to the findings about the design in the simulations.

Fig. 25 Comparison on part level by overlay of the actual flow front given by short shots molded in PP and the simulated flow front for the microfluidic mixer.

Fig. 26 Comparison on feature level between SEM picture of the actual flow front given by short shots molded in PP (left) and the simulated flow front (right) for the microfluidic mixer.

Table Caption List

Table 1 Simulation results for the three investigated gate types of the microfluidic distributor.

Table 2 Simulation results for the three investigated film gate thicknesses of the micro mixer.

FIGURES AND TABLES

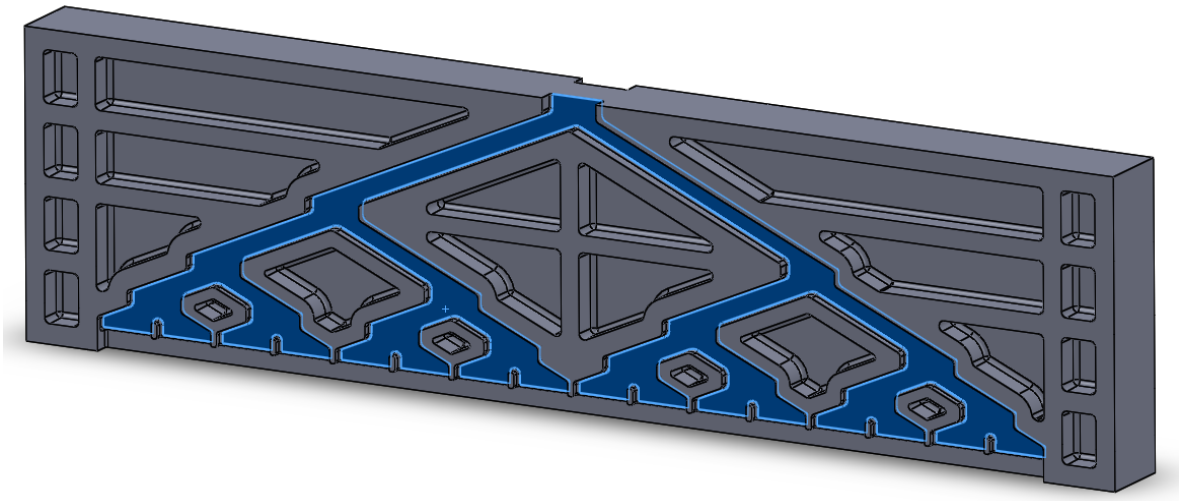

Fig. 1. CAD model of the first investigated micro plastic part with tree-like structure for the distribution of fluid (highlighted in blue color).

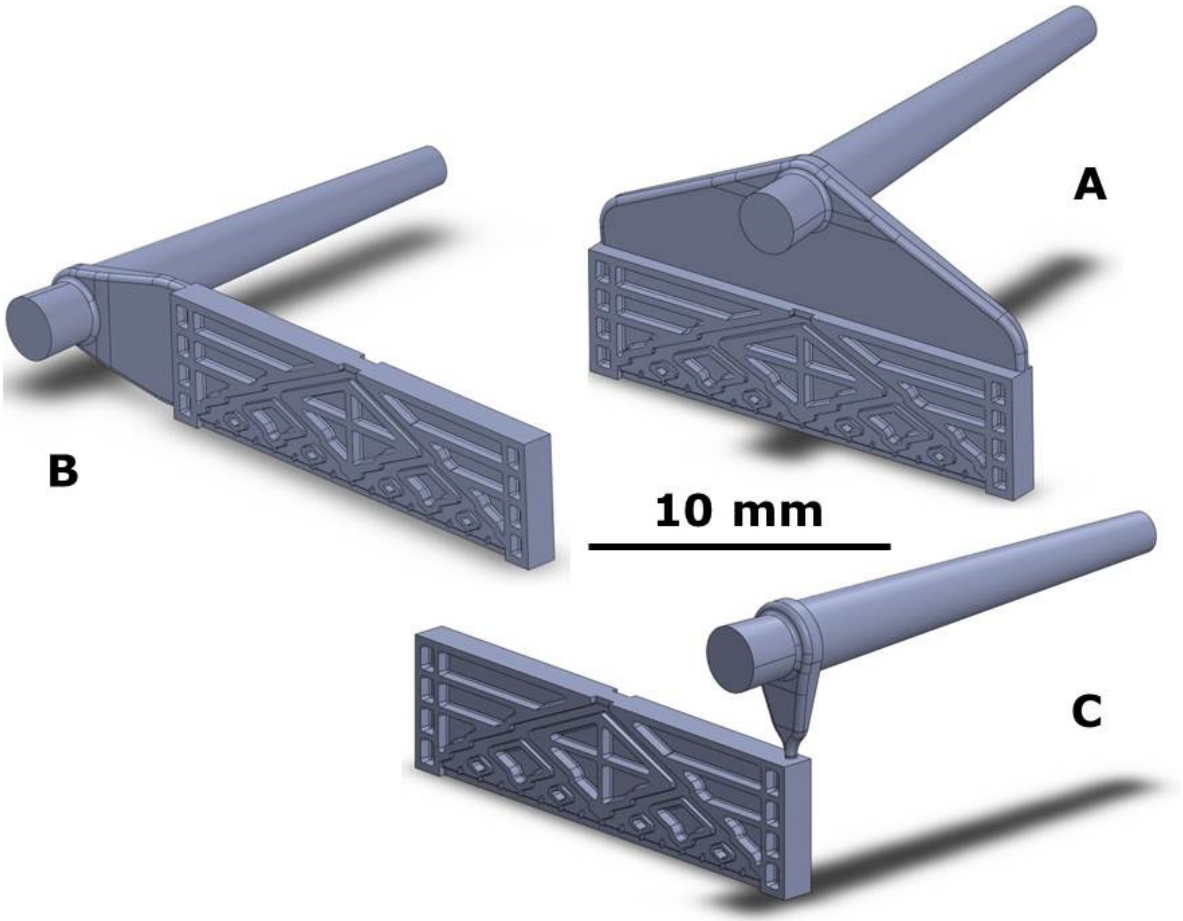

Fig. 2. CAD models of the microfluidic distributor with three different gate designs.
A: fan gate at long side (25 mm wide and 0.5 mm thick).
B: fan gate at short side (7 mm wide and 0.5 mm thick).
C: pin gate at long side (semi-circular, 0.5 mm diameter).

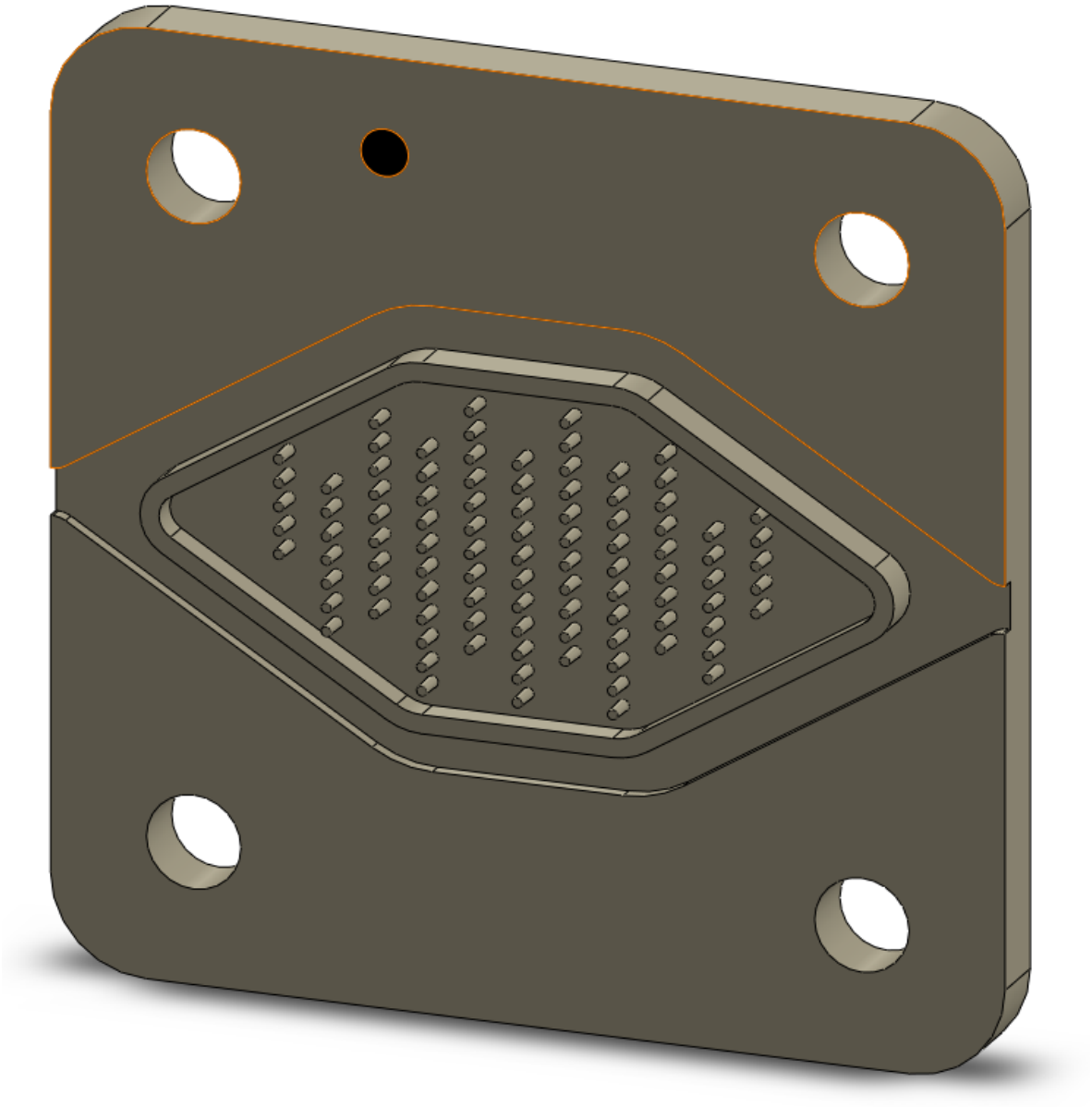

Fig. 3. CAD model of the second investigated micro plastic part which acts as microfluidic mixer.

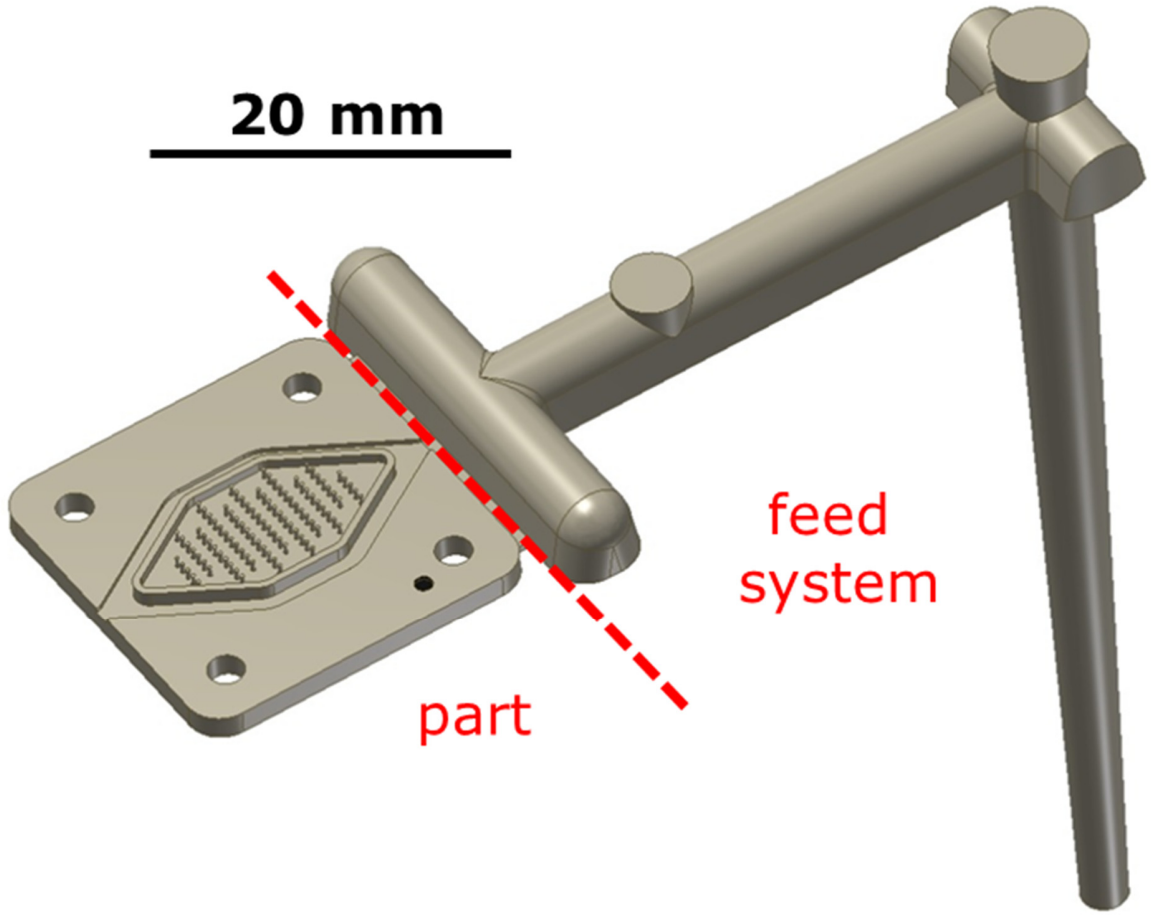

Fig. 4. CAD model of the second investigated micro plastic part with feed system (film gate, runner, sprue).

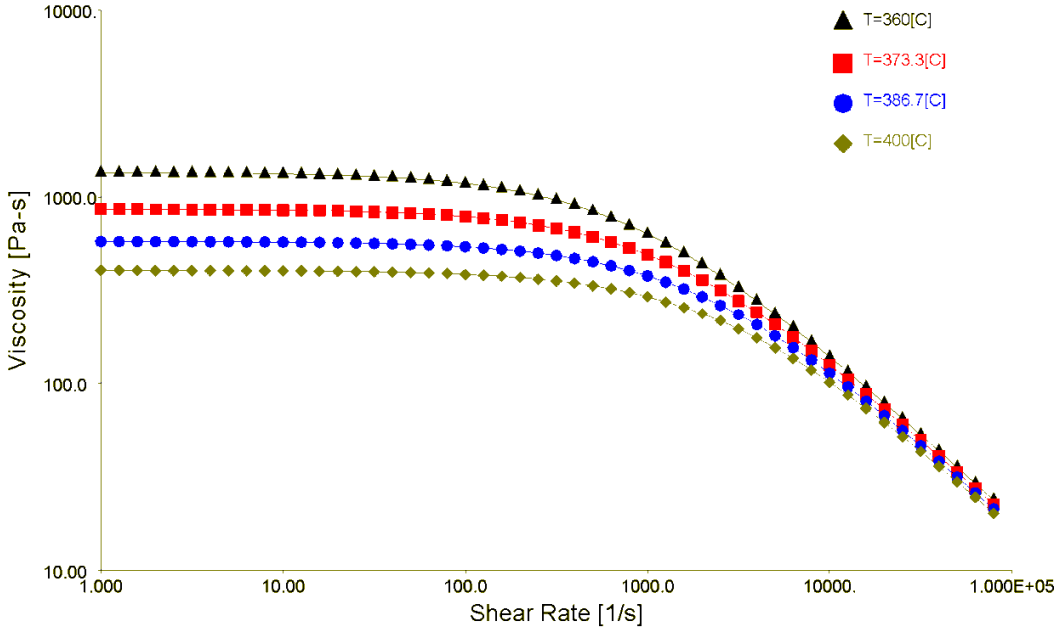

Fig. 5. Viscosity versus shear rate at different temperatures of the PEI Ultem 1000 which was used for the microfluidic manifold [26].

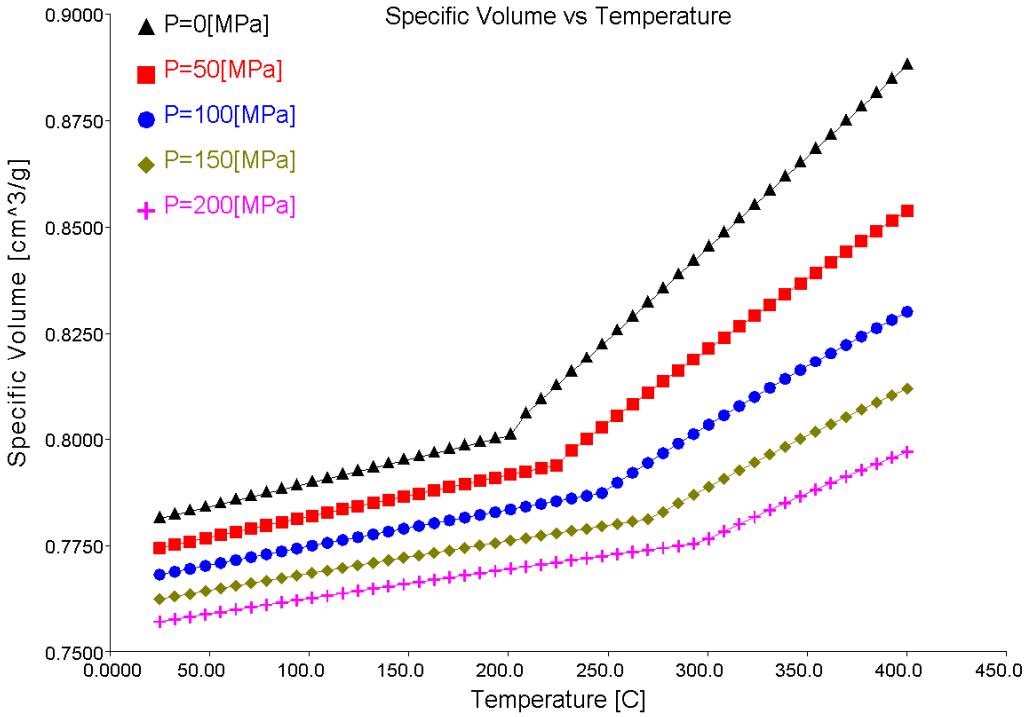

Fig. 6. pvT data at different pressure levels of the PEI Ultem 1000 which was used for the microfluidic manifold [26].

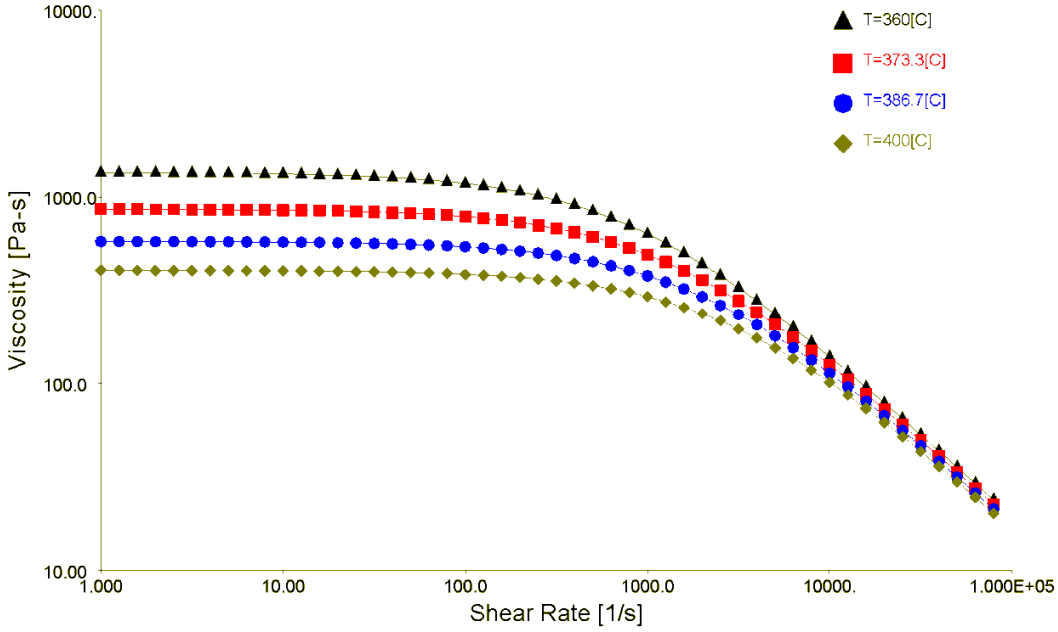

Fig. 7. Viscosity versus shear rate at different temperatures of the COC Topas 5013-L10 which was used for the microfluidic mixer [26].

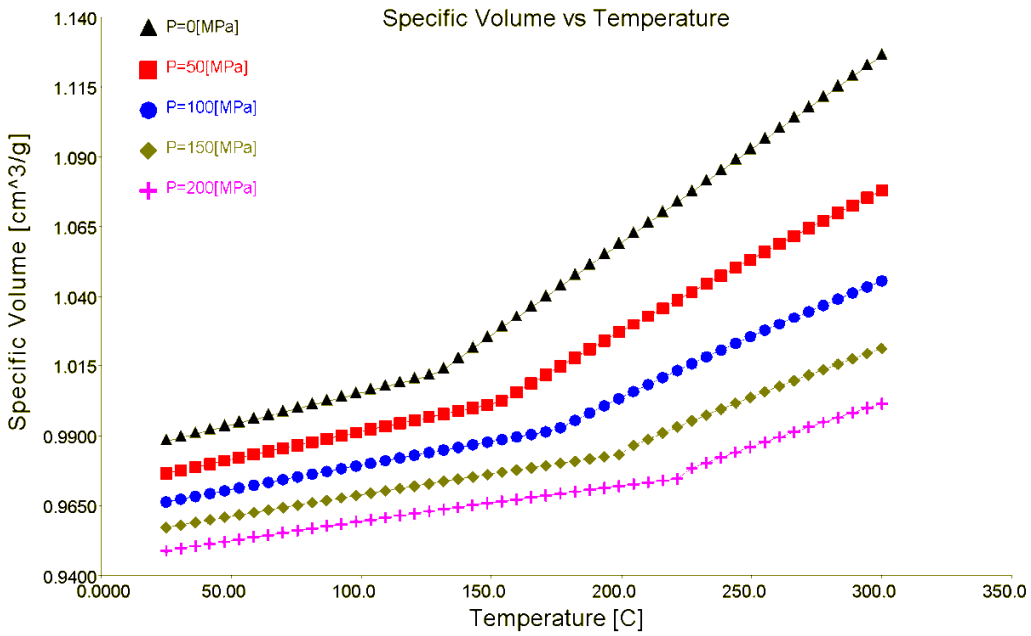

Fig. 8. pvT data at different pressure levels of the COC Topas 5013-L10 which was used for the microfluidic mixer [26].

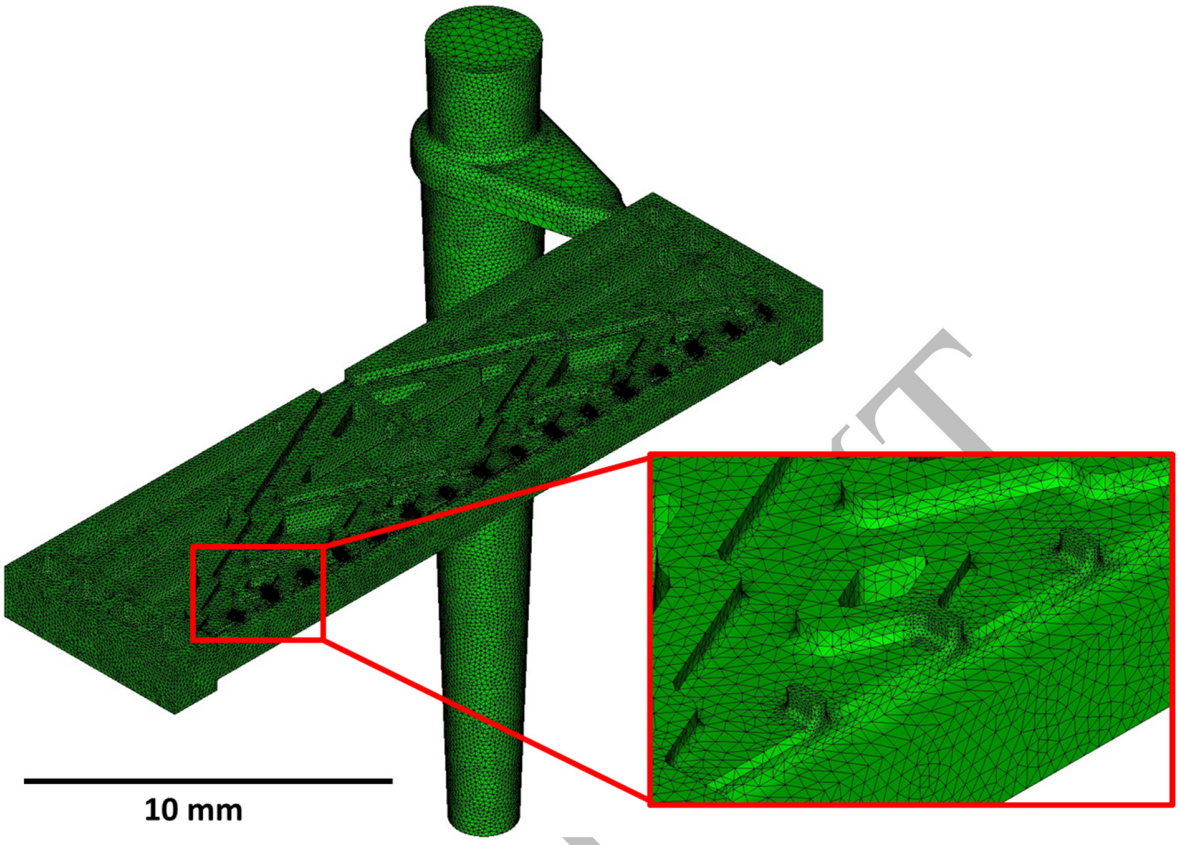

Fig. 9. Meshed micro distributor with closer view on some details (micro walls at outlets). Range of mesh edge length of the entire model: 40-800 µm.

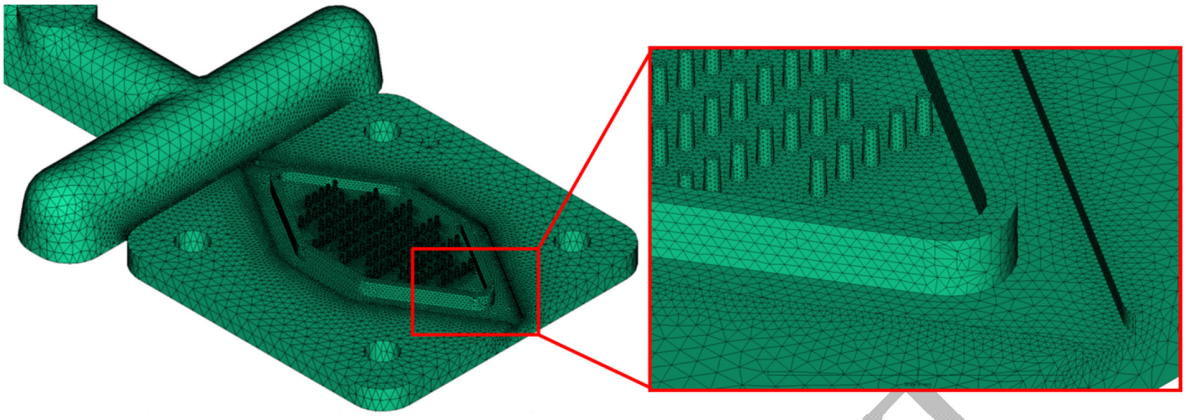

Fig. 10. Meshed micro mixer with closer view on some details (micro pillars and rim). Range of mesh edge length of the entire model: 65-800 µm.

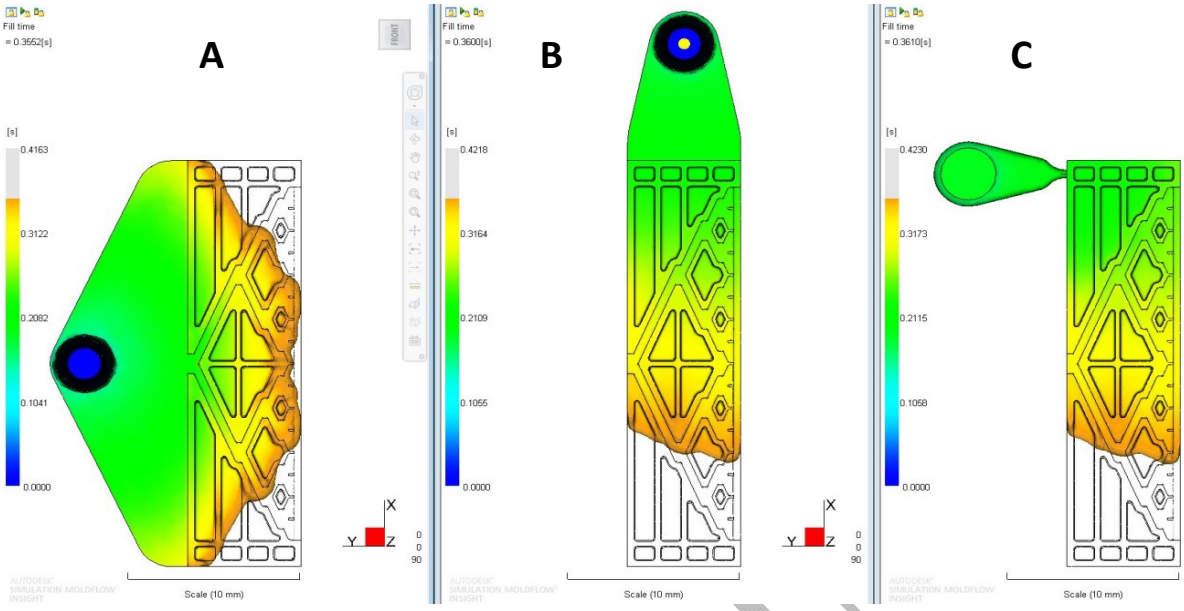

Fig. 11. Filling behavior for the three configurations of the fluidic distributor.

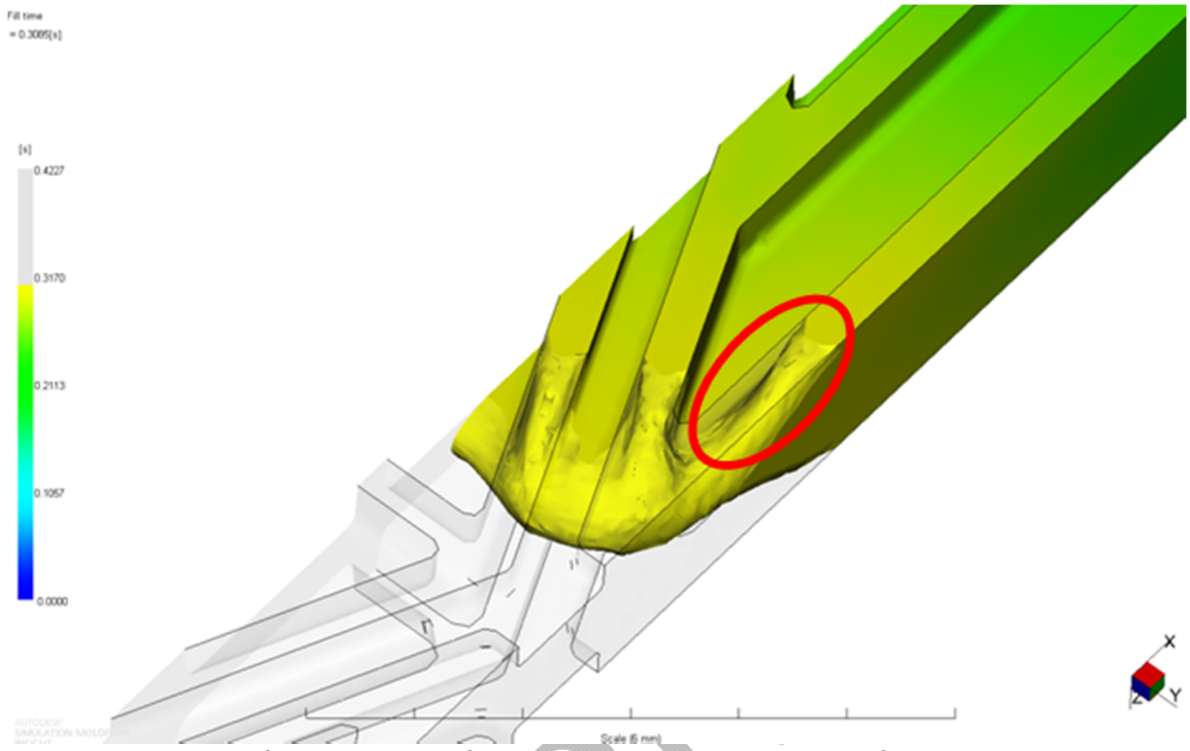

Fig. 12. Example of a rib acting as flow restrictors and causing the flow to lag behind compared to the bulk of the microfluidic distributor.

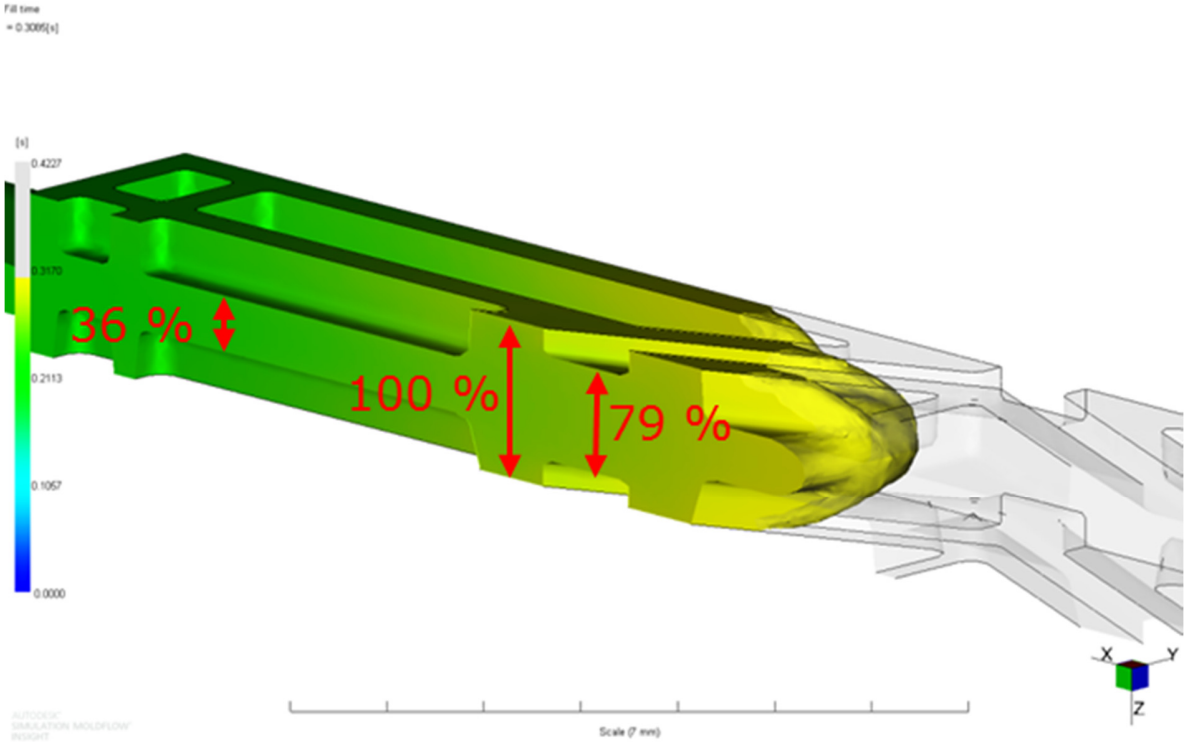

Fig. 13. Thickness variation in the part which contributes to the disturbance of the flow front in the cavity during the filling phase of the microfluidic distributor.

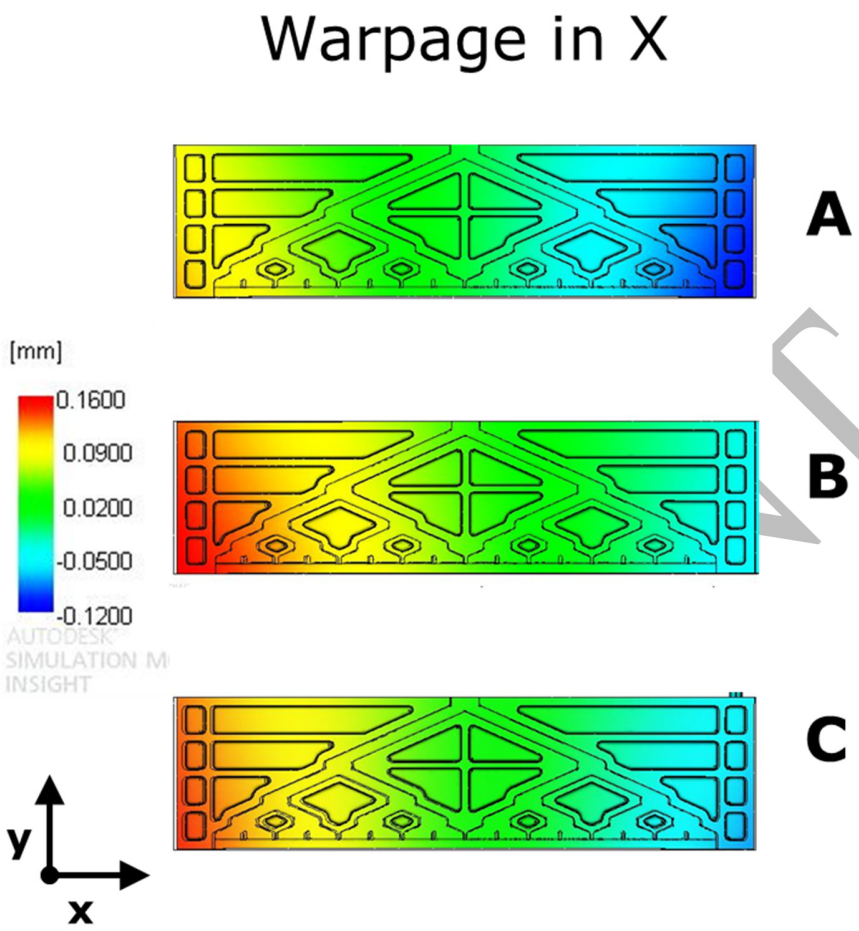

Fig. 14. Warpage prediction of the simulation in x direction for the micro fluidic distributor.

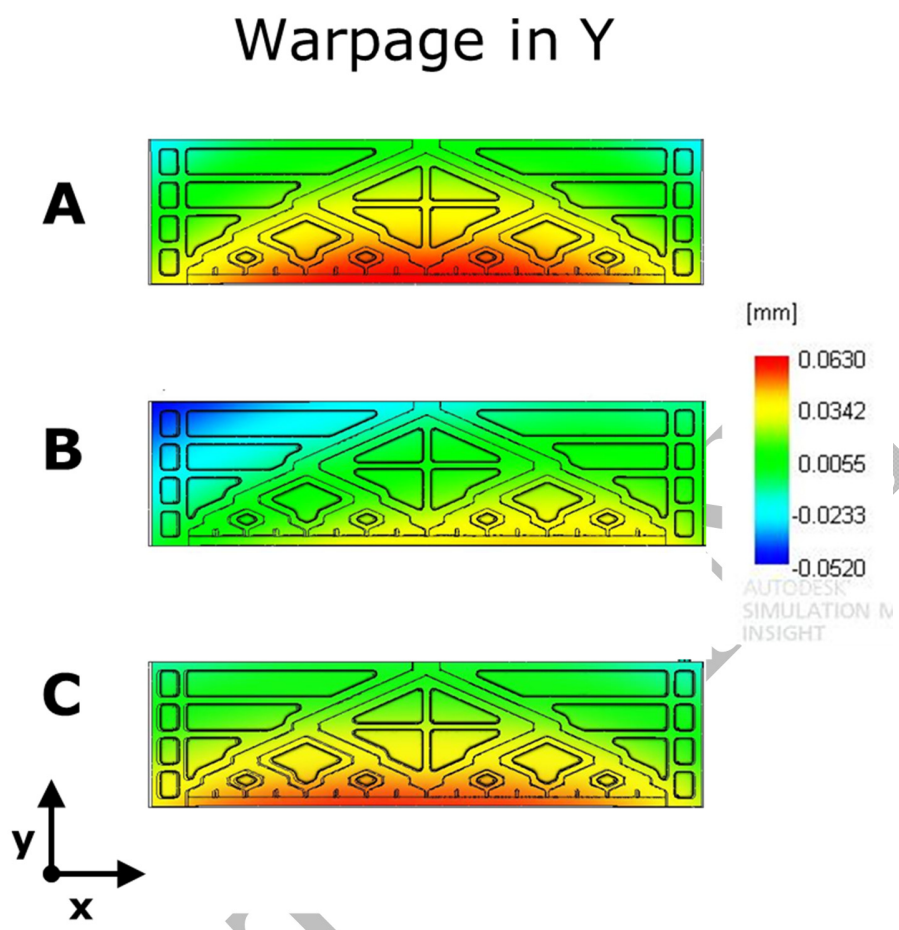

Fig. 15. Warpage prediction of the simulation in y direction for the micro fluidic distributor.

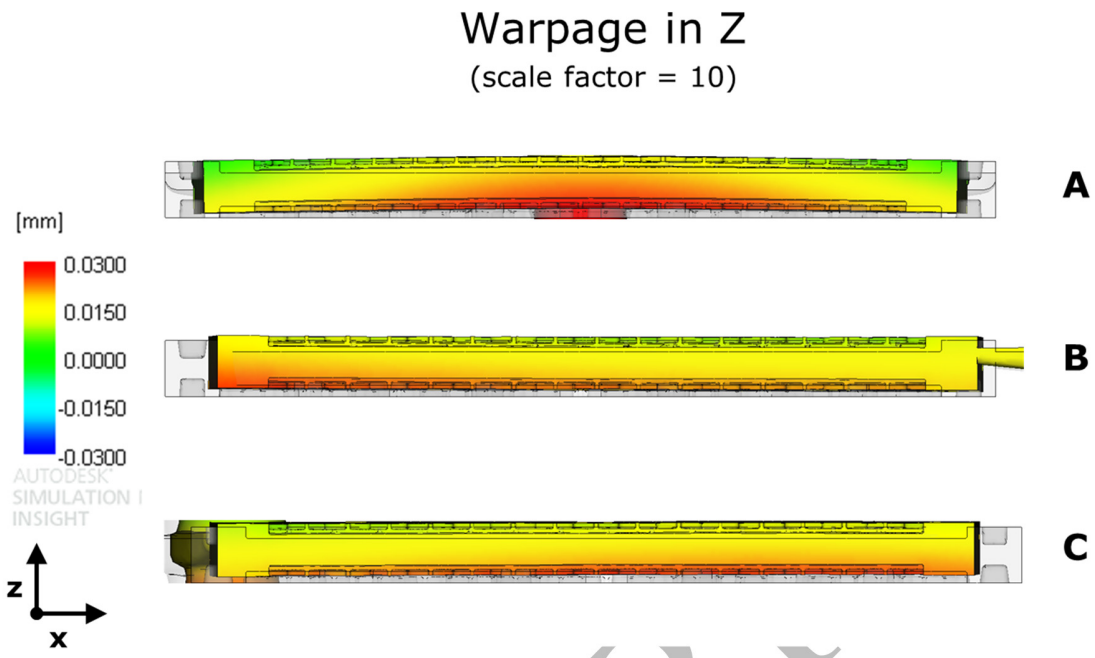

Fig. 16. Warpage prediction of the simulation in z direction for the micro fluidic distributor.

Fig. 17. Prediction of the warpage in z direction for the different gate sizes of gate design C (pin gate) of the microfluidic distributor.

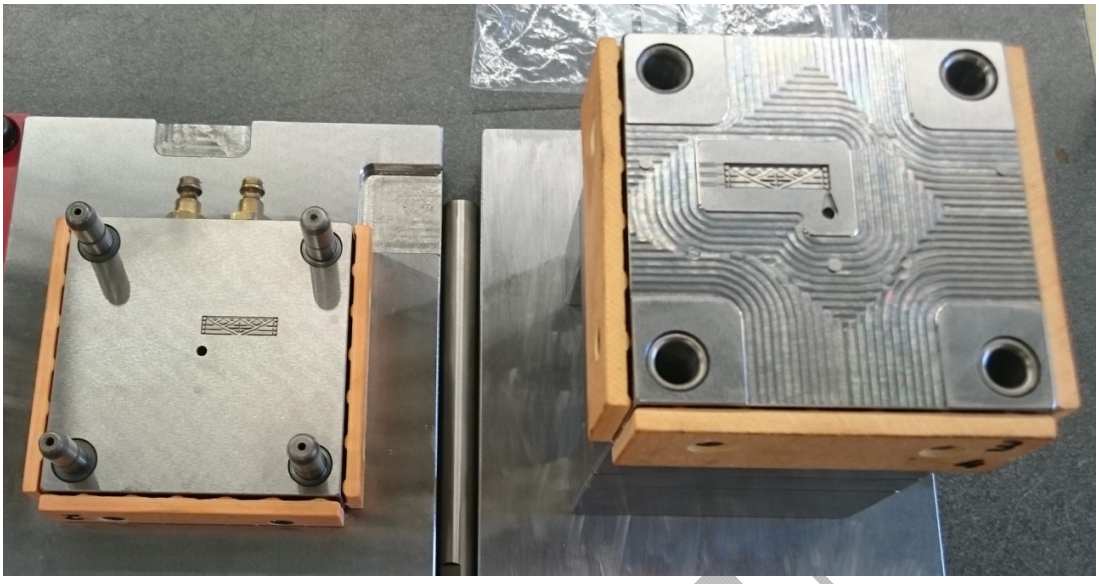

Fig. 18: Actual steel mold of the microfluidic manifold with stationary half (left) and the movable half (right). The cavity was machined according to the optimized design based on simulation results applying the insight from the simulations in practice.

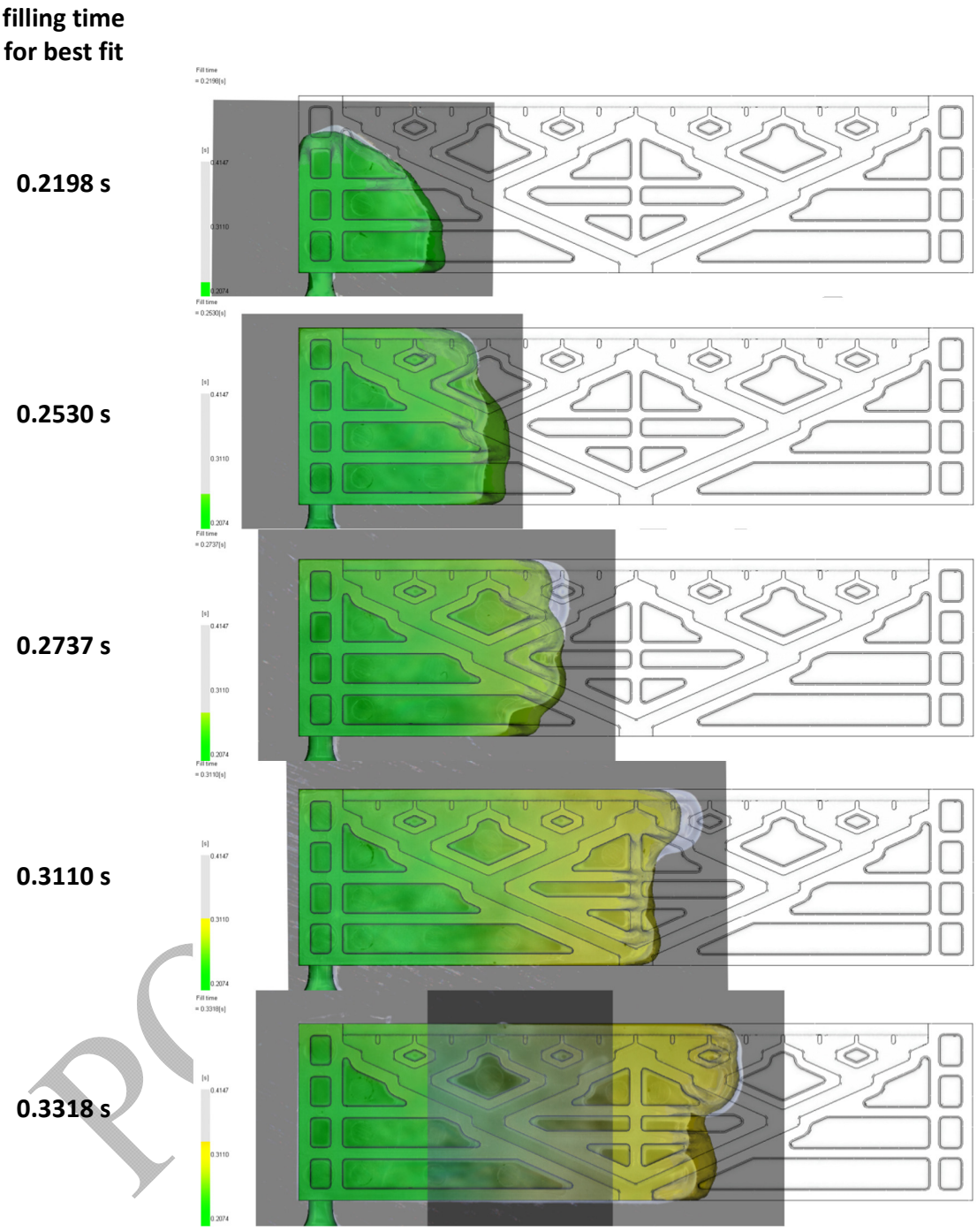

Fig. 19: Comparison on part level by overlay of the actual flow front given by short shots molded in PP and the simulated flow front for the microfluidic manifold.

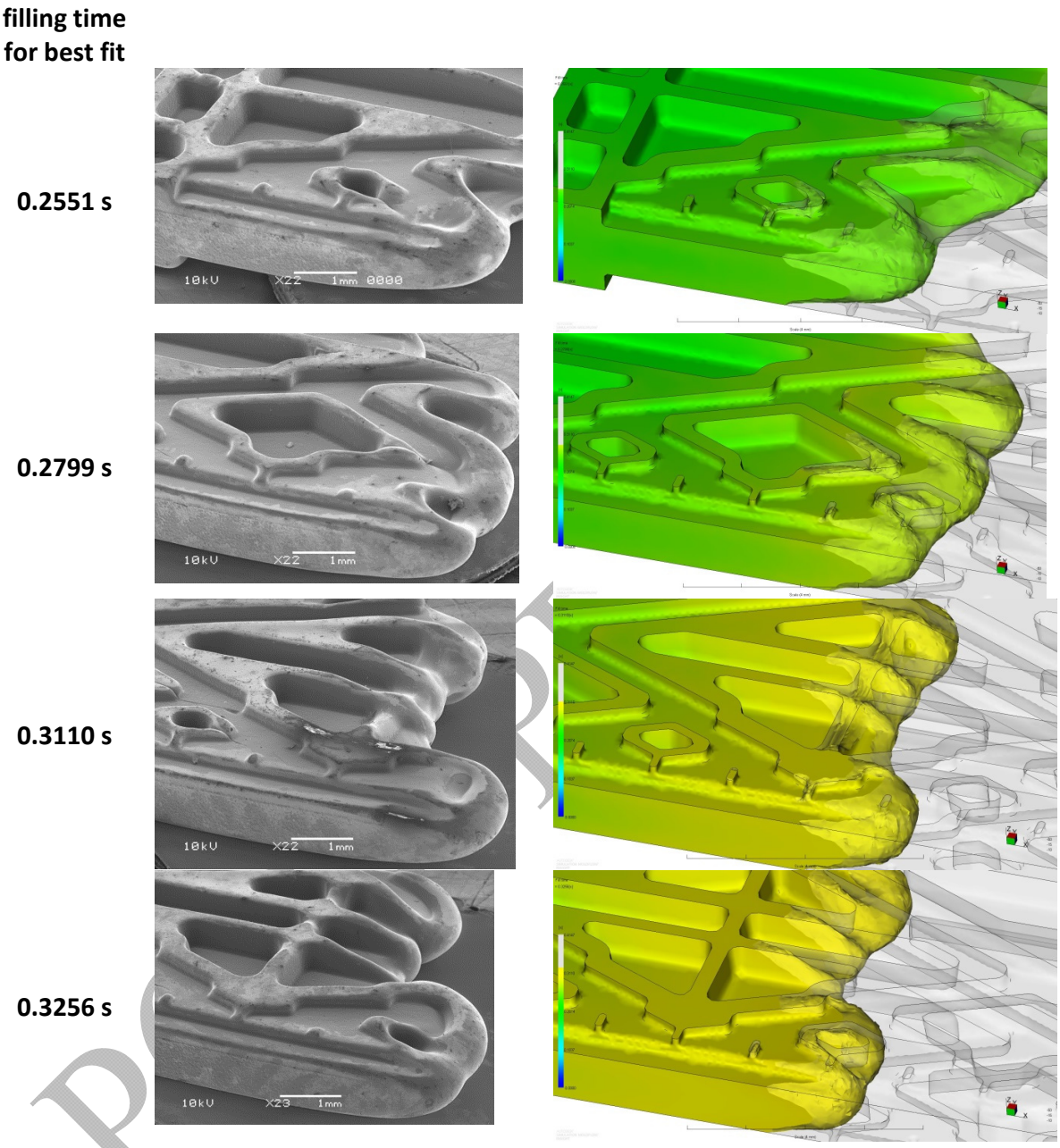

Fig. 20: Comparison on feature level between SEM picture of the actual flow front given by short shots in PP (left) and the simulated flow front (right) for the microfluidic manifold.

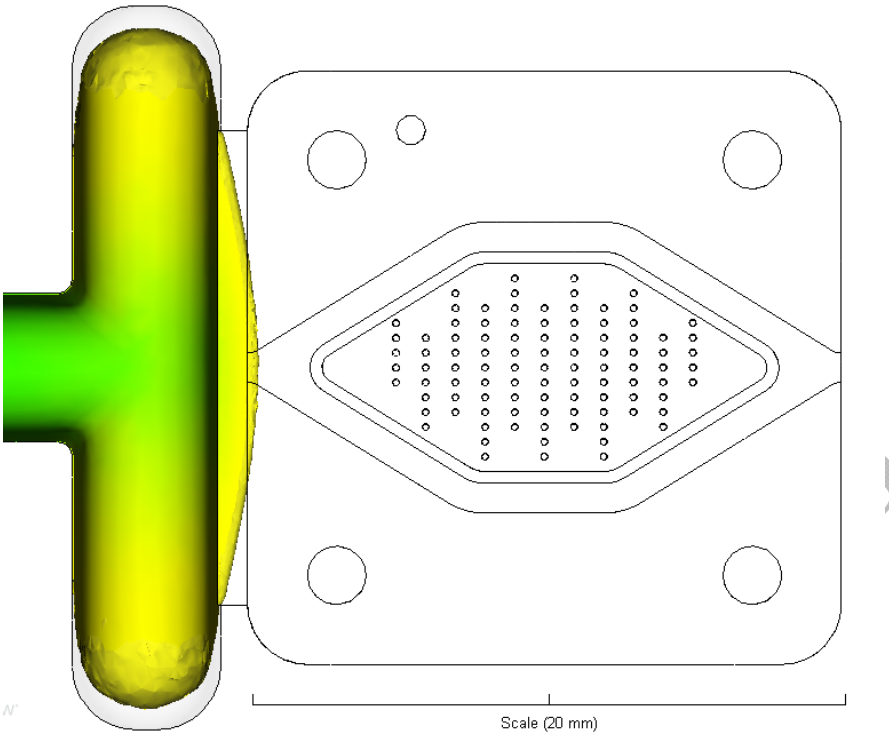

Fig. 21. Film gate of the microfluidic mixer with quite even flow front when the plastic is entering the actual part cavity.

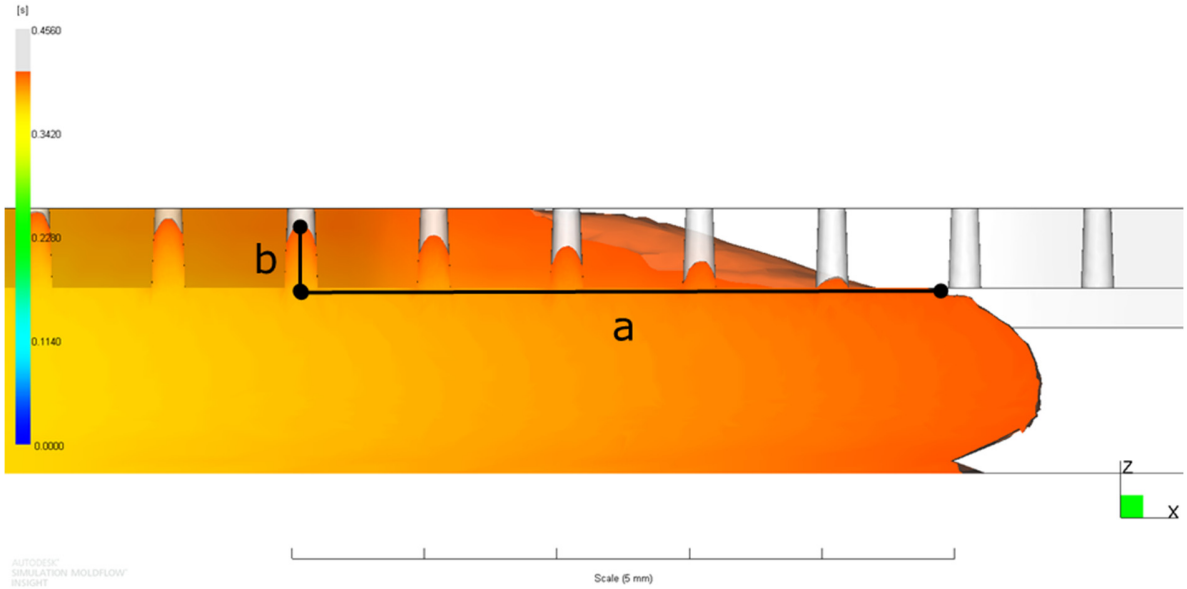

Fig. 22. Cross-sectional view of the flow in the microfluidic mixer with indication of the distinct hesitation effect at the micro pillars: the filling in bulk direction is faster than in the direction of the micro pillars, i.e. the flow length *a* in bulk direction is larger than the flow length *b* in direction of the micro pillars.

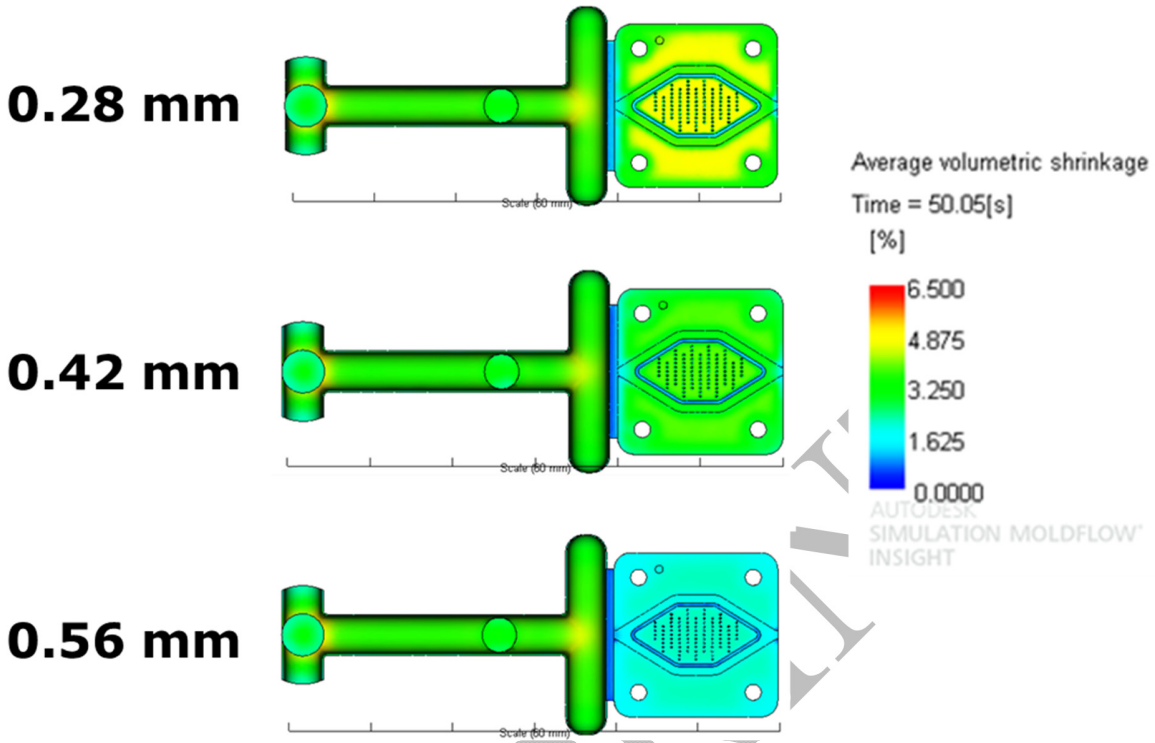

Fig. 23. Average volumetric shrinkage for the three film gates of the microfluidic mixer.

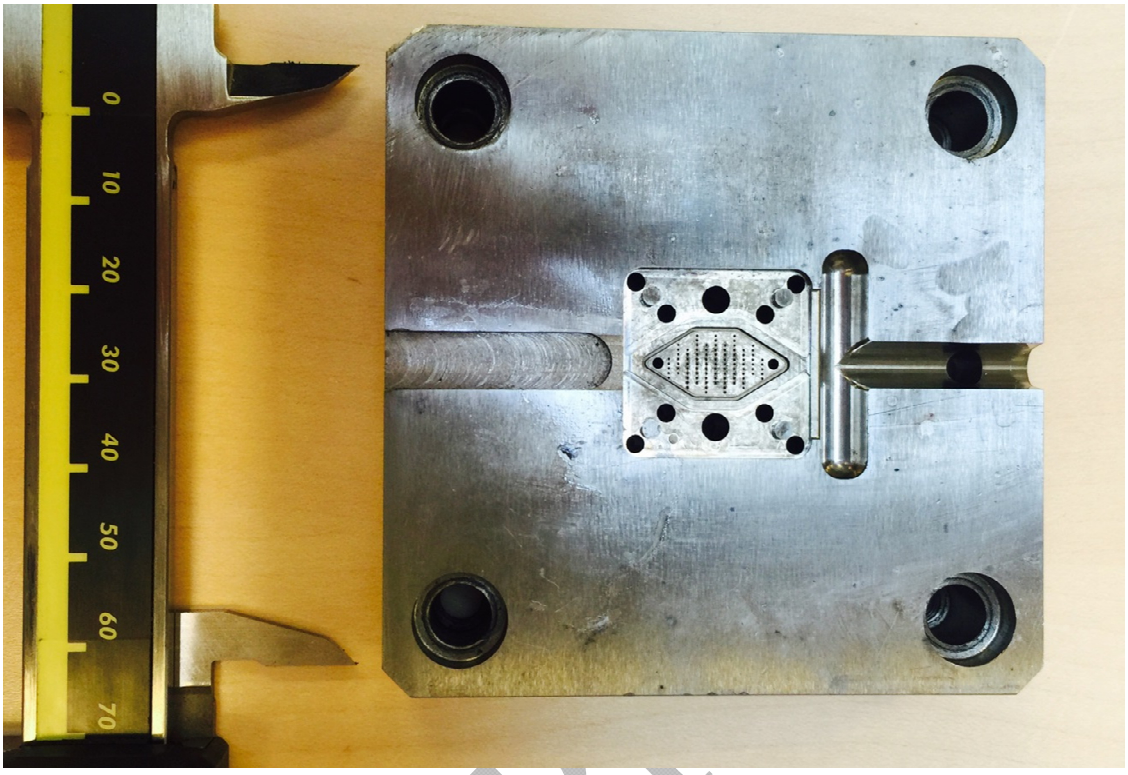

Fig. 24: Finished mold insert of the microfluidic mixer. The cavity design was machined accordingly to the findings about the design in the simulations.

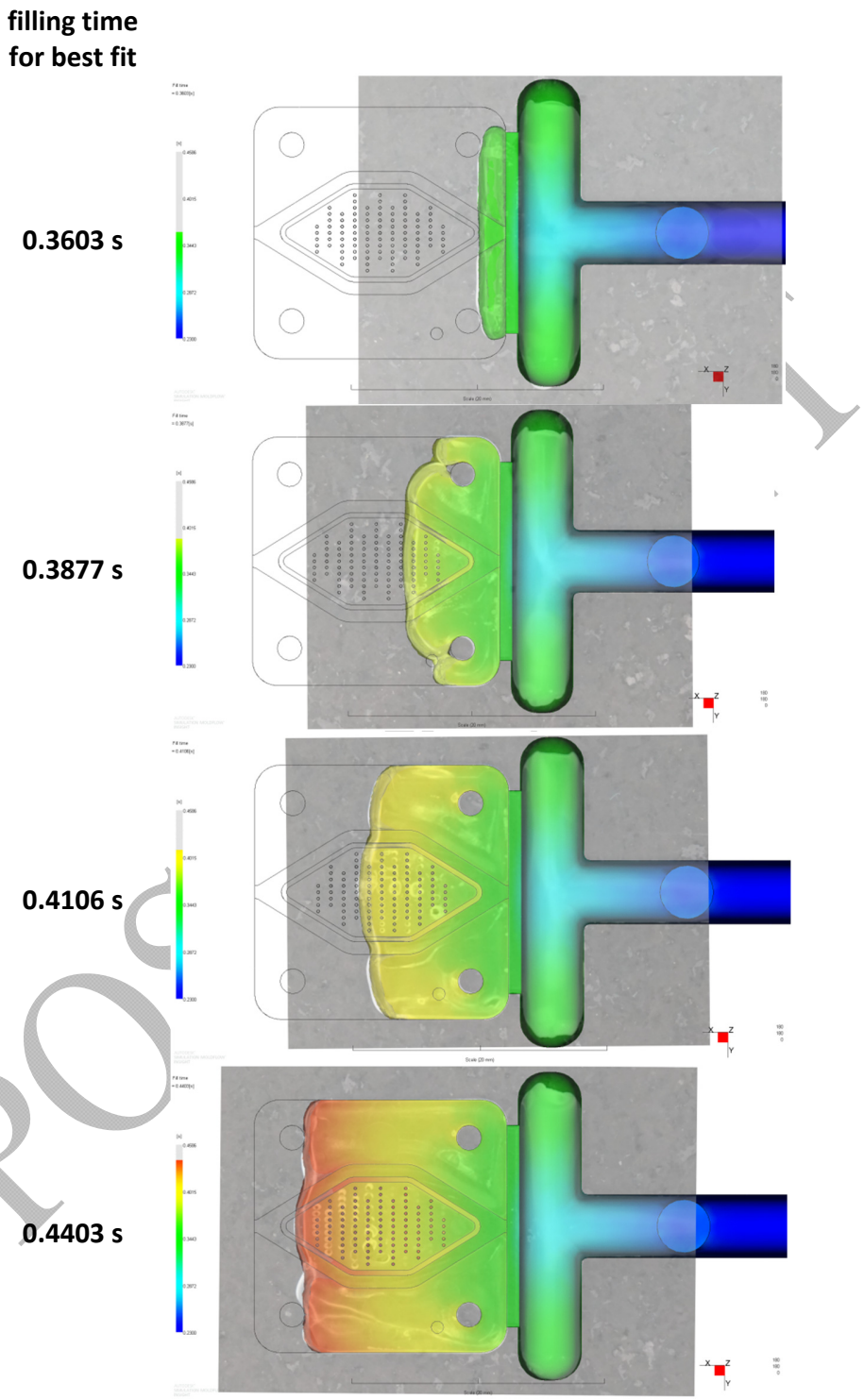

Fig. 25: Comparison on part level by overlay of the actual flow front given by short shots molded in PP and the simulated flow front for the microfluidic mixer.

filling time for best fit		
0.3832 s	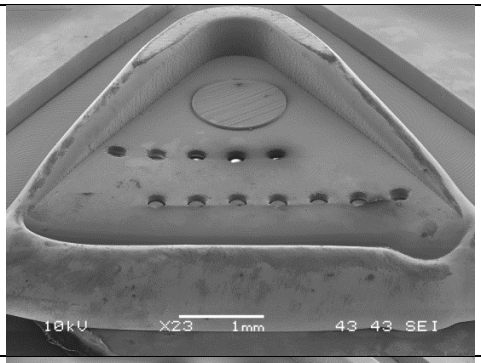	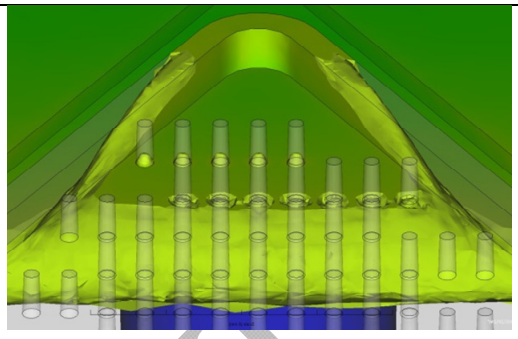
0.4083 s	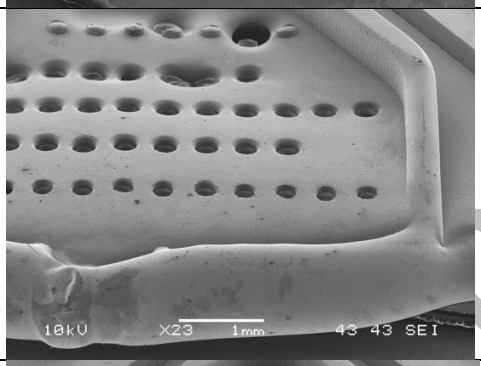	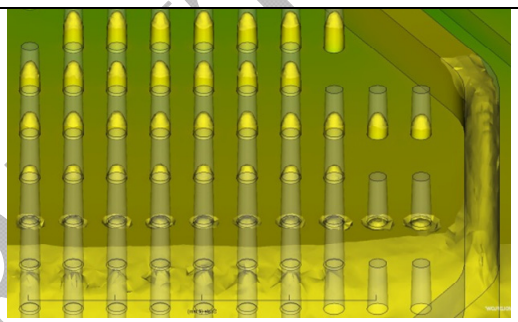
0.4380 s	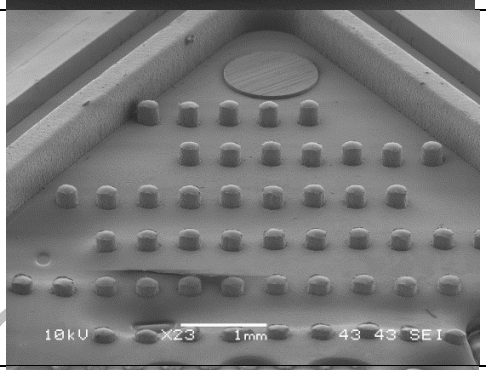	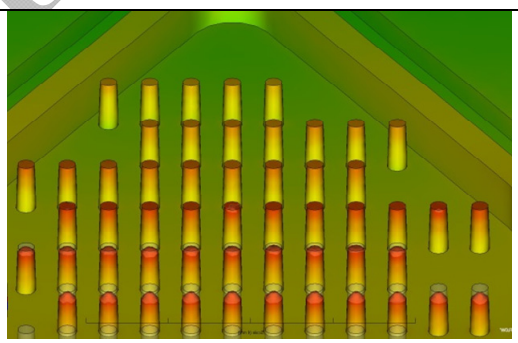
0.4578 s	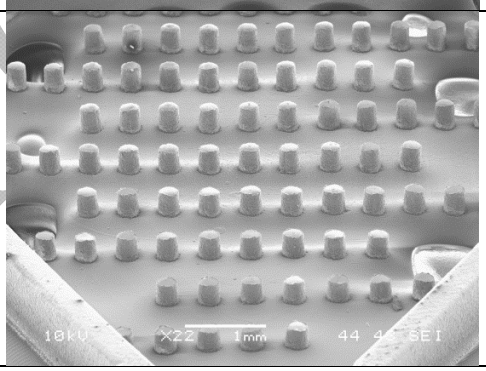	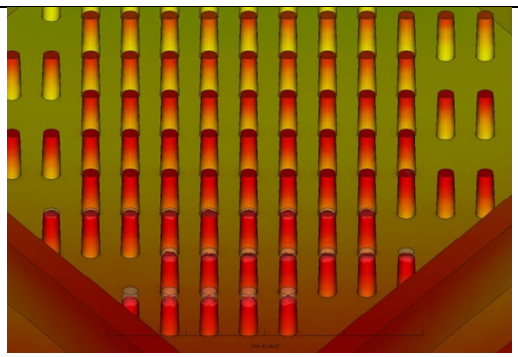

Fig. 26: Comparison on feature level between SEM picture of the actual flow front given by short shots molded in PP (left) and the simulated flow front (right) for the microfluidic mixer.

Table 1. Simulation results for the three investigated gate types of the microfluidic distributor.

Gate type	A	B	C	Limit
Max. injection pressure	50.7 MPa	78.8 MPa	94.7 MPa	250 MPa
Injection time	0.417 s	0.423 s	0.434 s	--
Max. clamp force	0.54 tons	0.69 tons	0.52 tons	60 tons
Average shrinkage	3.69 %	3.08 %	3.42 %	--
Max. shear rate	6 000 s^{-1}	8 000 s^{-1}	104 000 s^{-1}	50 000 s^{-1}
Flatness error	14 µm	14 µm	6 µm	10 µm

Table 2. Simulation results for the three investigated film gate thicknesses of the micro mixer.

Gate thickness	280 µm	420 µm	560 µm	Limit
Max. injection pressure	35.5 MPa	30.8 MPa	35.1 MPa	250 MPa
Max. clamp force	0.98 tons	1.21 tons	1.63 tons	60 tons
Part mass	2.221 g	2.229 g	2.237 g	2.317 g
Average shrinkage	3.16 %	2.93 %	2.68 %	--
Max. shear rate	411 000 s^{-1}	84 000 s^{-1}	52 000 s^{-1}	40 000 s^{-1}